

Chapter 11

Electroweak interactions

Literature:

- Böhm/Denner/Joos [11]

In this chapter a unified theory of electromagnetic and weak interactions is discussed. The energy scale of this unification corresponds to the mass of the vector bosons: $E_{\text{EW}} \sim M_W, M_Z \sim 100 \text{ GeV}$. At low energies, in contrast, there are two distinct interactions, the electromagnetic interaction described by QED, and the weak interaction described by Fermi's theory. Some signals are also present in low energy atomic physics, e. g. electroweak interference and parity violation.

11.1 Introduction – the weak force

A comparison of strong, electromagnetic and weak interactions is given in the following table:

Interaction	Involved	$\sim \tau/\text{s}$
Strong	quarks	10^{-23}
Electromagnetic	charged leptons and quarks	10^{-16}
Weak	all leptons and quarks	$10^{-6} - 10^{-8}$

One can observe that the timescales involved in weak decays are much larger than the ones of strong or electromagnetic decays. Thus, since $\tau \sim 1/\text{coupling}^2$, the weak coupling is supposed to be some orders of magnitude smaller than the strong coupling (see also Sect. 7.3.3).

Weak processes are classified according to the leptonic content of their final state:

- *Leptonic.*
E. g. $\mu^+ \rightarrow e^+ + \bar{\nu}_\mu + \nu_e$; $\nu_e + e^- \rightarrow \nu_e + e^-$.

- *Semi-leptonic.*
E. g. $\tau^+ \rightarrow \rho^+ + \bar{\nu}_\tau$.
- *Hadronic (non-leptonic).*
E. g. $K^0 \rightarrow \pi^+ + \pi^-$; $\Lambda^0 \rightarrow n + \pi^0$.

The weak interaction violates parity (P) and charge conjugation (C) symmetry. It also violates CP and T , much more weakly, though. Also flavor is not conserved in weak interactions (see Sect. 7.3.2). If $m_\nu \neq 0$, neutrino oscillations occur and lepton family number is not conserved either.

Let us review some of the experimental results for the weak interaction.

Existence of neutrinos. Consider nuclear β^- decay, assuming a two-particle final state: $n \rightarrow p + e^-$. Since $m_e \ll m_n, m_p$, the recoil can be neglected and so

$$\begin{aligned} m_n &= E_p + E_e \\ m_n &\simeq m_p + p_e \\ p_e &\simeq m_n - m_p. \end{aligned}$$

This result means that for a two-body decay monoenergetic electrons are to be expected. However, the measured electron spectrum is continuous (see Fig. 11.1(a)). To solve this problem, Fermi and Pauli introduced an invisible neutrino carrying part of the decay energy: $n \rightarrow p + e^- + \bar{\nu}_e$ (see Fig. 11.1(b)). The Fermi theory amplitude for this process reads

$$\mathcal{M} = \frac{G_F}{\sqrt{2}} (\bar{\psi}_p \gamma^\mu \psi_n) (\bar{\psi}_e \gamma_\mu \psi_{\bar{\nu}}), \quad (11.1)$$

where $G_F \sim 1/(300 \text{ GeV})^2$ is the Fermi constant. Note that the expression in Eq. (11.1) has vector structure and therefore does not violate parity. This point will be revisited later on.

Leptonic decays of π^\pm . Since π^\pm is the lightest hadron, it cannot decay into other hadrons. Furthermore, electromagnetic decay (like in the case of $\pi^0 \rightarrow \gamma\gamma$) is forbidden by charge conservation. Thus no other channels are obscuring the study of the leptonic decay $\pi^+ \rightarrow \mu^+ + \nu_\mu$.

Non-observation of $\mu \rightarrow e + \gamma$. Although energetically possible, the decay $\mu^- \rightarrow e^- + \gamma$ is not observed in experiment. This leads to the introduction of a new quantum number called lepton number L , where

$$\begin{aligned} L_l &= 1 & e^-, \mu^-, \nu_e, \dots \\ L_{\bar{l}} &= -1 & e^+, \mu^+, \bar{\nu}_e, \dots \end{aligned}$$

The leptonic muon decay conserving lepton number per family reads $\mu^- \rightarrow e^- + \nu_\mu + \bar{\nu}_e$.

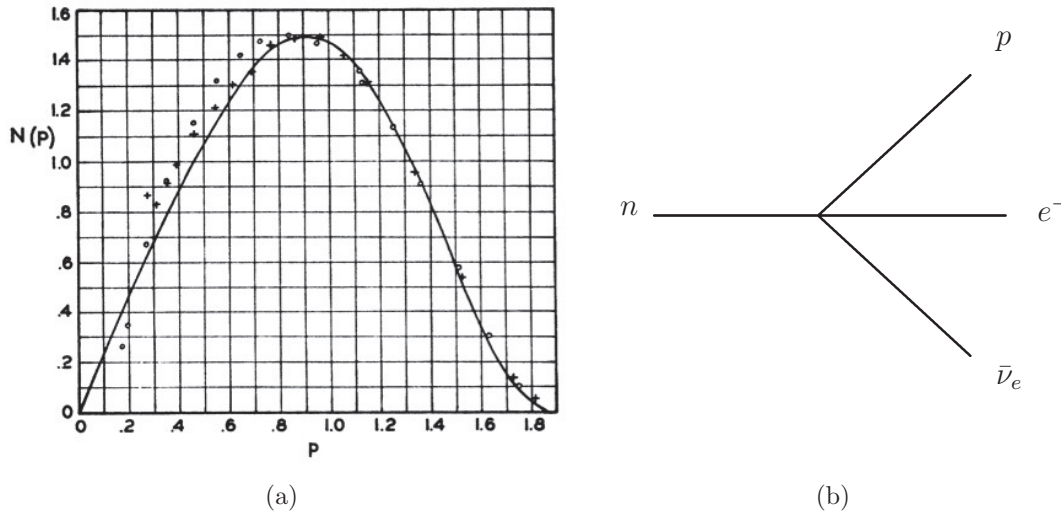


Figure 11.1: β^- decay spectrum (a) and diagram (b). (a) shows an electron momentum spectrum for the β^- decay of ^{64}Cu , source: [12, p. 14].

Parity violation. One famous instance of parity violation is the so-called τ - θ puzzle (1956). It consists in the finding that the Kaon K^+ decays into two final states with opposite parity:

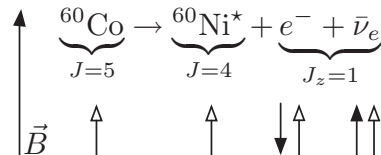
$$K^+ \begin{cases} \theta \rightarrow \pi^+ \pi^0 \\ \tau \rightarrow \pi^+ \pi^+ \pi^- \end{cases}$$

$$P |\pi\pi\rangle = (-1)(-1)(-1)^l = +1$$

$$P |\pi\pi\pi\rangle = (-1)^3 (-1)^{l_{\pi_1\pi_2}} (-1)^{l_{\pi_3}} = -1,$$

where l denotes angular momentum eigenvalues. The above is true for $J_{K^+} = 0$, since then, by conservation of angular momentum, $l = 0$ and $l_{\pi_1\pi_2} \oplus l_{\pi_3} = 0$ such that $l_{\pi_1\pi_2} = l_{\pi_3}$. Lee and Young introduced the idea that θ and τ are the same particle K^+ (fitting into its multiplet, see Fig. 7.6) which undergoes a flavor changing decay.

Another famous example for the demonstration of parity violation in weak interactions is the Wu experiment (1957). The idea is to consider β decay of nuclei polarized by an external magnetic field:



The Cobalt nuclei are aligned to the external magnetic field and are in a state with $J = 5$. By conservation of angular momentum, the electron and neutrino spins have to be parallel (the decay product ${}^{60}\text{Ni}^*$ is fixed). Since, to fulfill momentum conservation, they are emitted in opposite directions, the electron and its neutrino must have opposite

chirality. It is observed that electrons are emitted preferentially opposite to the \vec{B} field direction:

$$\begin{aligned} & \Gamma ({}^{60}\text{Co} \rightarrow {}^{60}\text{Ni}^* + e_L^- + \bar{\nu}_{e,R}) \\ & > \Gamma ({}^{60}\text{Co} \rightarrow {}^{60}\text{Ni}^* + e_R^- + \nu_{e,L}) = P \{ \Gamma ({}^{60}\text{Co} \rightarrow {}^{60}\text{Ni}^* + e_L^- + \bar{\nu}_{e,R}) \}. \end{aligned}$$

Thus left-handed leptons and right-handed antileptons ($e_L^-, \bar{\nu}_{e,R}$) are preferred over right-handed leptons and left-handed antileptons ($e_R^-, \bar{\nu}_{e,L}$). Recall (Sect. 5.2.4) that one uses the projectors $P_{R,L} = \frac{1}{2}(\mathbb{1} \pm \gamma_5)$ to indicate the chirality basis: $u_{L,R} = P_{L,R}u$.

These observations gave rise to the $V - A$ theory of weak interactions, described in Sect. 11.3 below.

11.2 γ_5 and $\varepsilon_{\mu\nu\rho\sigma}$

Recall that the amplitude in Eq. (11.1) does not violate parity. Therefore it has to be modified such that parity violation is included. To achieve this aim, the matrix γ^μ which forms the vector $\bar{\psi}\gamma^\mu\psi$ has to be replaced by a linear combination of elements of the set

$$\{\mathbb{1}, \gamma^\mu, \sigma^{\mu\nu}, \gamma_5\gamma^\mu, \gamma_5\}$$

where $\sigma^{\mu\nu} = \frac{i}{2}[\gamma^\mu, \gamma^\nu]$ and $\gamma_5 = i\gamma^0\gamma^1\gamma^2\gamma^3$. Using these matrices we can form the following field bilinears whose names are inspired by their transformation behavior under proper and improper Lorentz transformations¹

$\bar{\psi}\psi$	scalar
$\bar{\psi}\gamma^\mu\psi$	vector
$\bar{\psi}\sigma^{\mu\nu}\psi$	tensor
$\bar{\psi}\gamma_5\psi$	pseudoscalar
$\bar{\psi}\gamma^\mu\gamma_5\psi$	pseudovector.

In Sect. 5.2.4 we discussed operators on spinor spaces, including helicity,

$$h = \frac{1}{2}\vec{\sigma} \cdot \frac{\vec{p}}{|\vec{p}|} \otimes \mathbb{1} \qquad P_\pm = \frac{1}{2}(\mathbb{1} \pm h),$$

and chirality,

$$\gamma_5 \qquad P_{R,L} = \frac{1}{2}(\mathbb{1} \pm \gamma_5).$$

Recall that in the high energy limit chirality and helicity have the same eigenstates. The chirality matrix γ_5 has the following useful properties (see also Sect. 5.9)

¹See e. g. [13, p. 64].

- $\gamma_5^2 = \mathbb{1}$;
- $\{\gamma_5, \gamma_\mu\} = 0$;
- $\gamma_5^\dagger = i\gamma^3\gamma^2\gamma^1\gamma^0 = \gamma_5$;
- $\text{Tr}\gamma_5 = 0$;
- Dirac-Pauli representation: $\gamma_5 = \begin{pmatrix} 0 & \mathbb{1} \\ \mathbb{1} & 0 \end{pmatrix}$.

Now let us define the totally antisymmetric ε tensor in four dimensions:

$$\varepsilon^{\mu\nu\rho\sigma} = \begin{cases} +1, & \{\mu, \nu, \rho, \sigma\} \text{ even permutation of } \{0, 1, 2, 3\} \\ -1, & \{\mu, \nu, \rho, \sigma\} \text{ odd permutation of } \{0, 1, 2, 3\} \\ 0 & \text{else} \end{cases}, \quad (11.2)$$

such that

$$\begin{aligned} \varepsilon^{0123} &= +1 \\ \varepsilon^{\mu\nu\rho\sigma} &= -\varepsilon_{\mu\nu\rho\sigma}. \end{aligned}$$

The product of two such ε tensors is then given by

$$\varepsilon^{\mu\nu\rho\sigma} \varepsilon^{\mu'\nu'\rho'\sigma'} = -\det \begin{pmatrix} g^{\mu\mu'} & g^{\mu\nu'} & g^{\mu\rho'} & g^{\mu\sigma'} \\ g^{\nu\mu'} & g^{\nu\nu'} & g^{\nu\rho'} & g^{\nu\sigma'} \\ g^{\rho\mu'} & g^{\rho\nu'} & g^{\rho\rho'} & g^{\rho\sigma'} \\ g^{\sigma\mu'} & g^{\sigma\nu'} & g^{\sigma\rho'} & g^{\sigma\sigma'} \end{pmatrix}$$

resulting in

$$\begin{aligned} \varepsilon^{\mu\nu\rho\sigma} \varepsilon_{\mu\nu}{}^{\rho'\sigma'} &= -2(g^{\rho\rho'} g^{\sigma\sigma'} - g^{\rho\sigma'} g^{\sigma\rho'}) \\ \varepsilon^{\mu\nu\rho\sigma} \varepsilon_{\mu\nu\rho}{}^{\sigma'} &= -6g^{\sigma\sigma'} \\ \varepsilon^{\mu\nu\rho\sigma} \varepsilon_{\mu\nu\rho\sigma} &= -24 = -4!. \end{aligned}$$

Using the definition in Eq. (11.2), one can express γ_5 as

$$\gamma_5 = i\gamma^0\gamma^1\gamma^2\gamma^3 = -\frac{i}{4!}\varepsilon_{\mu\nu\rho\sigma}\gamma^\mu\gamma^\nu\gamma^\rho\gamma^\sigma.$$

Here are some traces involving γ_5 :

- $\text{Tr}\gamma_5 = 0$;
- $\text{Tr}(\gamma_5\gamma^\mu\gamma^\nu) = 0$;

- $\text{Tr}(\gamma_5 \gamma^\alpha \gamma^\beta \gamma^\gamma \gamma^\delta) = -4i \varepsilon^{\alpha\beta\gamma\delta}$
Observe that interchanging two matrices in the trace above yields a minus sign, furthermore the trace vanishes if two indices are identical. Hence the trace is proportional to the ε -tensor:

$$a \varepsilon^{\alpha\beta\gamma\delta} = \text{Tr}(\gamma_5 \gamma^\alpha \gamma^\beta \gamma^\gamma \gamma^\delta).$$

Multiplying both sides by $\varepsilon_{\alpha\beta\gamma\delta}$ yields

$$\begin{aligned} -24a &= \text{Tr}(\gamma_5 \gamma^\alpha \gamma^\beta \gamma^\gamma \gamma^\delta) \varepsilon_{\alpha\beta\gamma\delta} \\ &= 24i \text{Tr}(\gamma_5 \gamma_5 = \mathbb{1}) \\ \Rightarrow a &= -4i. \end{aligned}$$

11.3 The $V - A$ amplitude

The correct linear combination of bilinears replacing the vector $\bar{\psi} \gamma^\mu \psi$ in Eq. (11.1) in order to achieve parity violation turns out to be the “vector minus axialvector”, or $V - A$, combination $\bar{\psi} \gamma^\mu \psi - \bar{\psi} \gamma^\mu \gamma_5 \psi$.²

Adjusting the amplitude in Eq. (11.1) accordingly yields for the β^- decay amplitude

$$\mathcal{M}(n \rightarrow p e^- \bar{\nu}_e) = \frac{G_F}{\sqrt{2}} [\bar{u}_p \gamma^\mu (\mathbb{1} - \gamma_5) u_n] [\bar{u}_e \gamma_\mu (\mathbb{1} - \gamma_5) u_{\nu_e}] \quad (11.3)$$

and analogously for the muon decay

$$\mathcal{M}(\mu^- \rightarrow \nu_\mu e^- \bar{\nu}_e) = \frac{G_F}{\sqrt{2}} [\bar{u}_{\nu_\mu} \gamma^\mu (\mathbb{1} - \gamma_5) u_\mu] [\bar{u}_e \gamma_\mu (\mathbb{1} - \gamma_5) u_{\nu_e}]. \quad (11.4)$$

Let us analyze the general form and properties of $V - A$ amplitudes. Their structure is that of a current-current interaction:

$$\mathcal{M} = \frac{4}{\sqrt{2}} G_F J_i^\mu J_{j,\mu}^\dagger \quad (11.5)$$

where

$$J_i^\mu = \bar{u}_{i^0} \gamma^\mu \frac{1}{2} (\mathbb{1} - \gamma_5) u_{i^-} \quad (11.6)$$

$$J_{j,\mu}^\dagger = \bar{u}_{j^-} \gamma_\mu \frac{1}{2} (\mathbb{1} - \gamma_5) u_{j^0}. \quad (11.7)$$

Note the following properties of this kind of amplitudes:

²An axialvector is a pseudovector, since the prefix “pseudo” is used for cases where an extra minus sign arises under the parity transformation (in contrast to the non-pseudo case).

1. $\gamma^\mu(\mathbb{1} - \gamma_5)$ selects left-handed fermions,

$$\gamma_5 u_L = \gamma_5 P_L u = \gamma_5 \frac{1}{2}(\mathbb{1} - \gamma_5)u = -\frac{1}{2}(\mathbb{1} - \gamma_5)u = -u_L,$$

and right-handed antifermions, as desired.

2. G_F is universal.
3. Parity and charge conjugation alter the outcome of experiments, but here CP is conserved:

$$\begin{array}{lll} \Gamma(\pi^+ \rightarrow \mu_R^+ + \nu_L) \neq \Gamma(\pi^+ \rightarrow \mu_L^+ + \nu_R) & \not{P} & \times \\ \Gamma(\pi^+ \rightarrow \mu_R^+ + \nu_L) \neq \Gamma(\pi^- \rightarrow \mu_R^- + \bar{\nu}_L) & \not{C} & \times \\ \Gamma(\pi^+ \rightarrow \mu_R^+ + \nu_L) = \Gamma(\pi^- \rightarrow \mu_L^- + \bar{\nu}_R) & CP & \checkmark. \end{array}$$

11.4 Muon decay – determination of G_F

Consider the decay

$$\mu^-(p) \rightarrow e^-(p') + \bar{\nu}_e(k') + \nu_\mu(k),$$

see Fig. 11.2. The amplitude is given by

$$\mathcal{M} = \frac{G_F}{\sqrt{2}} [\bar{u}(k)\gamma^\mu(\mathbb{1} - \gamma_5)u(p)] [\bar{u}(p')\gamma_\mu(\mathbb{1} - \gamma_5)v(k')].$$

Recall that the differential decay rate reads

$$d\Gamma = \frac{1}{2E_\mu} |\mathcal{M}|^2 (2\pi)^4 dR_3(p', k, k')$$

where

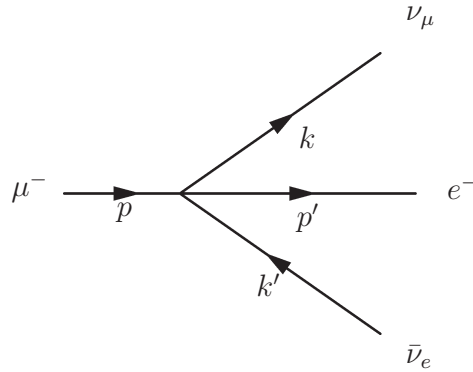
$$dR_3(p', k, k') = \frac{d^3p'}{(2\pi)^3 2E_{p'}} \frac{d^3k}{(2\pi)^3 2E_k} \frac{d^3k'}{(2\pi)^3 2E_{k'}} \delta^{(4)}(p - p' - k - k').$$

For $m_\nu = m_e = 0$ this yields

$$\frac{d\Gamma}{dE_{p'}} = \frac{m_\mu G_F^2}{2\pi^3} m_\mu^2 E_{p'}^2 \left(3 - \frac{4E_{p'}}{m_\mu} \right)$$

and

$$\Gamma = \int_0^{m_\mu/2} dE_{p'} \frac{d\Gamma}{dE_{p'}} = \frac{G_F^2 m_\mu^5}{192\pi^3} = \frac{1}{\tau}.$$

Figure 11.2: *Leptonic muon decay.*

The measured muon lifetime is

$$\tau = 2.1970 \cdot 10^{-6} \text{ s} = 2.9960 \cdot 10^{-10} \text{ eV};$$

assuming a muon mass of

$$m_\mu = 105.658 \cdot 10^6 \text{ eV},$$

this yields

$$G_F = 1.166 \cdot 10^{-5} \text{ GeV}^{-2} \simeq \frac{1}{(300 \text{ GeV})^2}$$

which is a dimensionful ($[G_F] = m^{-2}$) quantity. This hints to the fact that there are some problems with Fermi's theory:

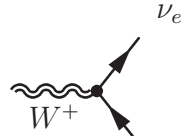
1. It deals with massless fermions only.
2. It is not renormalizable. This problem, along with the dimensionful coupling, is typical for an effective theory, a low energy approximation of a more general theory, in this case the GWS theory.
3. It violates unitarity at high energies. E. g. one finds that the cross section for electron-neutrino scattering is divergent for $E_{\text{CM}} \rightarrow \infty$:

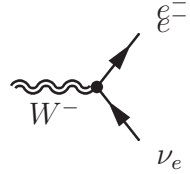
$$\sigma^{e^- + \nu_e \rightarrow e^- \nu_e} = \frac{4G_F^2}{\pi} E_{\text{CM}}^2.$$

One can show that the optical theorem yields the following unitarity constraint for the S -wave: $G_F^2 s^2 \lesssim 1$. Thus Fermi's theory is a good approximation only for $\sqrt{s} \lesssim 1/\sqrt{G_F}$ and it breaks down for higher energies.

11.5 Weak isospin and hypercharge

From the earlier analysis, we consider the currents of the weak interaction as charged currents³,

$$j_\mu = j_\mu^+ = \bar{u}_\nu \gamma_\mu \frac{1}{2}(1 - \gamma_5)u_e = \bar{\nu} \gamma_\mu \frac{1}{2}(1 - \gamma_5)e = \bar{\nu}_L \gamma_\mu e_L =$$


$$j_\mu^\dagger = j_\mu^- = \bar{u}_e \gamma_\mu \frac{1}{2}(1 - \gamma_5)u_\nu = \bar{e} \gamma_\mu \frac{1}{2}(1 - \gamma_5)\nu = \bar{e}_L \gamma_\mu \nu_L =$$


These currents correspond to transitions between pairs of fermions whose charge differs by one unit. For this reason, one speaks of **charged currents** (CC). These two currents are the ones associated with (weak) decays of muons and neutrons.

In analogy to the case of isospin, where the proton and neutron are considered as the two isospin eigenstates of the nucleon, we postulate a **weak isospin** doublet structure ($T = \frac{1}{2}$),

$$\chi_L = \begin{pmatrix} \nu \\ e \end{pmatrix}_L \quad \begin{matrix} T_3 = +\frac{1}{2} \\ T_3 = -\frac{1}{2} \end{matrix}, \quad (11.8)$$

with raising and lowering operators,

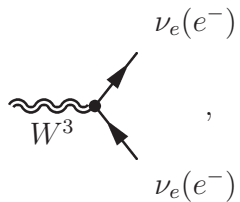
$$\tau_\pm = \frac{1}{2}(\tau_1 \pm i\tau_2),$$

where the τ_i are the usual Pauli matrices. With this formalism, one can write the charged currents as,

$$j_\mu^+ = \bar{\chi}_L \gamma_\mu \tau_+ \chi_L \quad (11.9)$$

$$j_\mu^- = \bar{\chi}_L \gamma_\mu \tau_- \chi_L \quad (11.10)$$

The next step consists in *postulating* an $SU(2)$ symmetry of these currents. In the case of isospin, this leads to the prediction of three currents mediated by the pions π^\pm, π^0 . We thus expect a third current to exist, which does not change the charge and is thus called **neutral current** (NC),

$$j_\mu^3 = \bar{\chi}_L \gamma_\mu \frac{1}{2} \tau_3 \chi_L = \bar{\nu}_L \gamma_\mu \frac{1}{2} \nu_L - \bar{e}_L \gamma_\mu \frac{1}{2} e_L =$$


$$, \quad (11.11)$$

³The 'plus' + and 'dagger' † shall not be confused.

yielding a weak isospin triplet of weak currents,

$$j_\mu^i = \bar{\chi}_L \gamma_\mu \frac{1}{2} \tau_i \chi_L \quad i = 1, 2, 3,$$

with algebra,

$$[\tau_i, \tau_j] = i \varepsilon_{ijk} \tau_k.$$

Now, we compare these to the electromagnetic current,

$$j_\mu^{em} = \bar{e} \gamma_\mu Q e = \bar{e}_R \gamma_\mu Q e_R + \bar{e}_L \gamma_\mu Q e_L, \quad (11.12)$$

where Q is the electromagnetic charge operator. This current is invariant under $U(1)_Q$, the gauge group of QED associated to the electromagnetic charge. It is however not invariant under the $SU(2)_L$ which we postulated for the weak currents : it contains e_L instead of χ_L .

To solve this issue, we construct an $SU(2)_L$ -invariant $U(1)$ -current,

$$j_\mu^Y = \bar{e}_R \gamma_\mu Y_R e_R + \bar{\chi}_L \gamma_\mu Y_L \chi_L, \quad (11.13)$$

where the **hypercharges** Y_R and Y_L are the conserved charge operators associated to the $U(1)_Y$ symmetry. It is different for left and right handed leptons.

We now want to write j_μ^{em} as a linear combination of j_μ^3 and $\frac{1}{2} j_\mu^Y$ (the factor $\frac{1}{2}$ is a matter of convention). One gets,

$$\bar{e}_R \gamma_\mu Q e_R + \bar{e}_L \gamma_\mu Q e_L = \bar{\nu}_L \gamma_\mu \frac{1}{2} \nu_L - \bar{e}_L \gamma_\mu \frac{1}{2} e_L + \frac{1}{2} \bar{e}_R \gamma_\mu Y_R e_R + \frac{1}{2} \bar{\chi}_L \gamma_\mu Y_L \chi_L,$$

from which we read out,

$$Y_R = 2Q \quad Y_L = 2Q + 1. \quad (11.14)$$

with the weak isospin third components,

$$\left. \begin{array}{l} T_3(e_R) = 0 \quad \text{singlet, blind to the weak interaction} \\ T_3(\nu_L) = +\frac{1}{2} \\ T_3(e_L) = -\frac{1}{2} \end{array} \right\} \text{doublet,}$$

one can then write the relation,

$$\boxed{Y = 2Q - 2T_3}. \quad (11.15)$$

In Tab. 11.1 and 11.2, we summarise the quantum numbers of leptons and quarks. It should be noted that the right handed neutrino ν_R does not carry $SU(2)_L$ or $U(1)_Y$ charges, and thus decouples from the electroweak interaction.

	T	T_3	Q	Y
ν_L	1/2	1/2	0	-1
e_L^-	1/2	-1/2	-1	-1
ν_R	0	0	0	0
e_R^-	0	0	-1	-2

Table 11.1: Weak quantum numbers of leptons

	T	T_3	Q	Y
u_L	1/2	1/2	2/3	1/3
d_L	1/2	-1/2	-1/3	1/3
u_R	0	0	2/3	4/3
d_R	0	0	-1/3	-2/3

Table 11.2: Weak quantum numbers of quarks

11.6 Construction of the electroweak interaction

As in the case of QED (Sec. 5.12, p.98) and QCD (Sec. 7.4, p. 138), we expect the electroweak interaction to be mediated by gauge fields. In the case of QED, we had,

$$\mathcal{L}_{int}^{\text{QED}} = -iej_\mu^{em} A^\mu,$$

where e is the $(U(1)_Q)$ -coupling, j_μ^{em} the $(U(1)_Q)$ -current, and A^μ the $(U(1)_Q)$ -gauge field (photon). We copy this for the current triplets and singlet :

$$\mathcal{L}_{int}^{\text{EW}} = -igj_\mu^i W^{i\mu} - i\frac{g'}{2}j_\mu^Y B^\mu, \quad (11.16)$$

where we introduced the $SU(2)_L$ -gauge field triplet $W^{i\mu}$ and singlet B^μ associated to the weak isospin and weak hypercharge respectively.

From those we can construct the massive charged vector bosons,

$$W^{\pm\mu} = \frac{1}{\sqrt{2}}(W^{1\mu} \mp iW^{2\mu}),$$

as well as the neutral vector bosons (mass eigenstates) as a linear combination of $W^{3\mu}$ and B^μ ,

$$\begin{aligned} A^\mu &= B^\mu \cos \theta_w + W^{3\mu} \sin \theta_w && \text{massless} \rightarrow \gamma, \\ Z^\mu &= -B^\mu \sin \theta_w + W^{3\mu} \cos \theta_w && \text{massive} \rightarrow Z^0, \end{aligned}$$

where θ_w is called the **weak mixing angle** (or sometimes Weinberg angle).

Substituting these quantities in the interaction Lagrangian of the neutral electroweak current, we obtain,

$$\begin{aligned} -igj_\mu^3 W^{3\mu} - i\frac{g'}{2}j_\mu^Y B^\mu &= -i \left(g \sin \theta_w j_\mu^3 + g' \cos \theta_w \frac{j_\mu^Y}{2} \right) A^\mu \\ &\quad - i \left(g \cos \theta_w j_\mu^3 - g' \sin \theta_w \frac{j_\mu^Y}{2} \right) Z^\mu. \end{aligned}$$

The first term corresponds to the electromagnetic current, for which we had $j_\mu^{em} = j_\mu^3 + \frac{1}{2}j_\mu^Y$, implying,

$$\boxed{g \sin \theta_w = g' \cos \theta_w = e}, \quad (11.17)$$

and thus linking the three couplings together. One often uses e and $\sin \theta_w$ as parameters for the standard model to be measured experimentally.

The second term corresponds to the weak neutral current. From $j_\mu^Y = 2(j_\mu^{em} - j_\mu^3)$, we get,

$$j_\mu^{\text{NC}} = \frac{g}{\cos \theta_w} (j_\mu^3 - \sin^2 \theta_w j_\mu^{em}). \quad (11.18)$$

11.7 Electroweak Feynman rules

Vertices The Feynman rules for vertices stemming from,

$$\mathcal{L}_{int}^{\text{EW}} = \mathcal{L}_{int}^{\text{QED}} + \mathcal{L}_{int}^{\text{CC}} + \mathcal{L}_{int}^{\text{NC}},$$

can be computed as follows,

$$\begin{aligned}
i\mathcal{L}_{int}^{\text{QED}} &= -ie\bar{\psi}_f\gamma_\mu Q\psi_f A^\mu \\
\Rightarrow & \text{Diagram: } \begin{array}{c} f \\ \nearrow \\ \text{---}\gamma\text{---} \\ \searrow \\ f \end{array} = -ieQ_f\gamma_\mu \\
i\mathcal{L}_{int}^{\text{CC}} &= -i\frac{g}{\sqrt{2}}(\bar{\chi}_L\gamma_\mu\tau_+\chi_L)W^{+\mu} - i\frac{g}{\sqrt{2}}(\bar{\chi}_L\gamma_\mu\tau_-\chi_L)W^{-\mu} \\
&= -i\frac{g}{\sqrt{2}}\bar{\nu}\gamma_\mu\left(\frac{1-\gamma_5}{2}\right)eW^{+\mu} - i\frac{g}{\sqrt{2}}\bar{e}\gamma_\mu\left(\frac{1-\gamma_5}{2}\right)\nu W^{-\mu} \\
\Rightarrow & \text{Diagram: } \begin{array}{c} \nu_e \\ \nearrow \\ \text{---}W^+\text{---} \\ \searrow \\ f \end{array} = \text{Diagram: } \begin{array}{c} e^- \\ \nearrow \\ \text{---}W^-\text{---} \\ \searrow \\ \nu_e \end{array} = -i\frac{g}{\sqrt{2}}\gamma_\mu\left(\frac{1-\gamma_5}{2}\right) \\
i\mathcal{L}_{int}^{\text{NC}} &= -i\frac{g}{\cos\theta_w}\bar{\psi}_f\gamma_\mu\left[\left(\frac{1-\gamma_5}{2}\right)T_3 - \sin^2\theta_w Q\right]\psi_f Z^\mu \\
&= -i\frac{g}{\cos\theta_w}\bar{\psi}_f\gamma_\mu\frac{1}{2}(c_V^f - c_A^f\gamma_5)\psi_f Z^\mu \\
\Rightarrow & \text{Diagram: } \begin{array}{c} f \\ \nearrow \\ \text{---}Z^0\text{---} \\ \searrow \\ f \end{array} = -i\frac{g}{\cos\theta_w}\gamma_\mu\frac{1}{2}(c_V^f - c_A^f\gamma_5)
\end{aligned}$$

where c_V^f and c_A^f are the vector and axial vector couplings of the fermion type f . A simple calculation yields,

$$c_V^f = T_3^f - 2\sin^2\theta_w Q^f \quad (11.19)$$

$$c_A^f = T_3^f. \quad (11.20)$$

Tab. 11.3 lists the couplings for the various types of fermions.

	Q^f	c_V^f	c_A^f
ν	0	1/2	1/2
e	-1	$-1/2 + 2\sin^2\theta_w$	-1/2
u	2/3	$1/2 - 4/3\sin^2\theta_w$	1/2
d	-1/3	$-1/2 + 2/3\sin^2\theta_w$	-1/2

Table 11.3: Vector and axial vector couplings of fermions.

Propagator of a massive vector boson Form Eq. (11.17), we see that e and g should be of the same order of magnitude (since we know experimentally that $\sin^2 \theta_w \approx 0.23$). This leads to the question : why is the weak interaction so much weaker than the electromagnetic one? This can be made evident by looking at the typical lifetime of weakly decaying particles (as the neutron or the muon) compared with electromagnetic decays. The answer lies in the large mass of the weak gauge bosons W^\pm and Z^0 .

The components $X^\mu = W^{+\mu}, W^{-\mu}, Z^\mu$ fulfill the Klein-Gordon equation,

$$(\square + M^2)X^\mu = 0, \quad \partial_\mu X^\mu = 0 \text{ (gauge fixing),}$$

which results in the propagator,

$$i \frac{\sum_\lambda (\varepsilon_\lambda^\mu)^* \varepsilon_\lambda^\nu}{p^2 - M^2}.$$

The polarisation sum $\Pi^{\mu\nu}$ must take the form,

$$\Pi^{\mu\nu} = \sum_\lambda (\varepsilon_\lambda^\mu)^* \varepsilon_\lambda^\nu = Ag^{\mu\nu} + Bp^\mu p^\nu.$$

Using the identities,

$$p_\mu p^\mu = M^2, \quad p_\mu \Pi^{\mu\nu} = p_\nu \Pi^{\mu\nu} = 0, \quad g_{\mu\nu} \Pi^{\mu\nu} = 3,$$

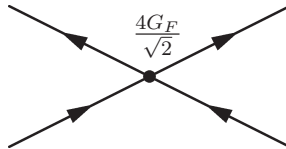
coming from the on-shell condition, the conservation of current and the count of polarization states (for a massive particle) respectively, we get $A = -1$ and $B = M^{-2}$, making us able to write,

$$\mu \text{ --- } \text{wavy line} \text{ --- } \nu = i \frac{-g^{\mu\nu} + p^\mu p^\nu / M^2}{p^2 - M^2}.$$

W^\pm, Z^0

So unless momentum transfer is not of the order of $M \gtrsim 100 \text{ GeV}$, the propagator gets suppressed drastically by the mass.

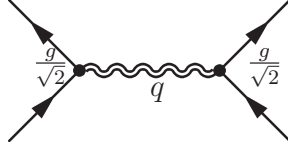
Relation of the Fermi $V - A$ -interaction In $V - A$ -theory, we have a 4 point vertex,



yielding the matrix element,

$$\mathcal{M}^{V-A} = \frac{4G_F}{\sqrt{2}} j^\mu j_\mu^\dagger.$$

The same process, viewed as the exchange of a low momentum ($q^2 \ll M_W^2$) vector boson,



corresponds to the matrix element,

$$\mathcal{M}^{\text{EW}} \approx \left(\frac{g}{\sqrt{2}} j^\mu \right) \frac{1}{M_W^2} \left(\frac{g}{\sqrt{2}} j_\mu^\dagger \right),$$

yielding the relation,

$$\boxed{G_F = \frac{\sqrt{2}g^2}{8M_W^2}}. \quad (11.21)$$

From this relation, the first estimates of the mass of the W^\pm bosons were 50 – 100 GeV.

11.8 Spontaneous symmetry breaking: Higgs mechanism

The ad hoc introduction of non-vanishing vector boson masses runs into a serious problem: One would have to include into the Lagrangian the usual mass term

$$\mathcal{L}_M = -\frac{m^2}{2} A_\mu A^\mu \quad (11.22)$$

which violates gauge invariance (the boson field transforms as $A_\mu \rightarrow A_\mu - \partial_\mu \alpha(x)$). If the “massive vector bosons” are indeed to be massive, gauge symmetry needs to be broken in some way, since the inclusion of a mass term requires breaking of gauge symmetry. To avoid problems at the theory level caused by broken gauge symmetry, the idea is to retain gauge symmetry in this respect, while physical states are less symmetric than the Lagrangian. This situation can e.g. also be found in solid state physics: Consider a ferromagnet modeled as a collection of spins. As long as no magnetization is imposed, this system is rotationally invariant. A non-vanishing magnetization breaks this symmetry, in

that it singles out a specific direction. Symmetry breaking occurs due to the influence of changing a continuous parameter (magnetization) caused by the environment. This does not affect the rotational invariance of the theory describing the ferromagnet and two physical states with different imposed directions are related by a transformation corresponding to the symmetry that is broken by imposing directions.

Let us start out with an example: Consider a real scalar field with a four-point interaction (which is to the complex scalar field what is the Ising model to the isotropic ferromagnet mentioned above):

$$\mathcal{L} = \frac{1}{2}(\partial_\mu\phi)^2 - \left(\frac{1}{2}\mu^2\phi^2 + \frac{1}{4}\lambda\phi^4\right) \quad (11.23)$$

$$= T - V \quad (11.24)$$

where $-1/2\mu^2\phi^2$ is a mass term and $-1/4\lambda\phi^4$ is an interaction term corresponding to the four-point vertex. Because the potential needs to be bounded from below, $\lambda > 0$. Observe that \mathcal{L} is even in ϕ and therefore invariant under the transformation $\phi \rightarrow -\phi$.

The vacuum state of this theory corresponds to a minimum of the potential:

$$\frac{\partial V}{\partial\phi} = \phi(\mu^2 + \lambda\phi^2) \stackrel{!}{=} 0. \quad (11.25)$$

Depending on the sign of μ^2 , one can distinguish two cases.

a) $\mu^2 > 0, \lambda > 0$.

In this case the vacuum state is reached for $\phi = 0$, see Fig. 11.3(a).

b) $\mu^2 < 0, \lambda > 0$.

Here, $\phi = 0$ is still an extremum, but has turned into a local maximum. In addition there are two minima at

$$\phi = \pm\sqrt{\frac{-\mu^2}{\lambda}} = \pm v$$

which correspond to two vacua, degenerate in energy, see Fig. 11.3(b). In this case, the symmetry transformation $\phi \rightarrow -\phi$, which leaves the Lagrangian in Eq. (11.23) invariant, changes two distinct physical states into each other.

A perturbative calculation is an expansion around the vacuum state. If we consider case b), this means $\phi = v$ or $\phi = -v$. Therefore, the symmetry $\phi \rightarrow -\phi$ is broken, although the Lagrangian has this symmetry irrespective of the signs of μ^2 and λ . Let us choose the positive sign vacuum state and expand:

$$\phi(x) = v + \eta(x) \quad (11.26)$$

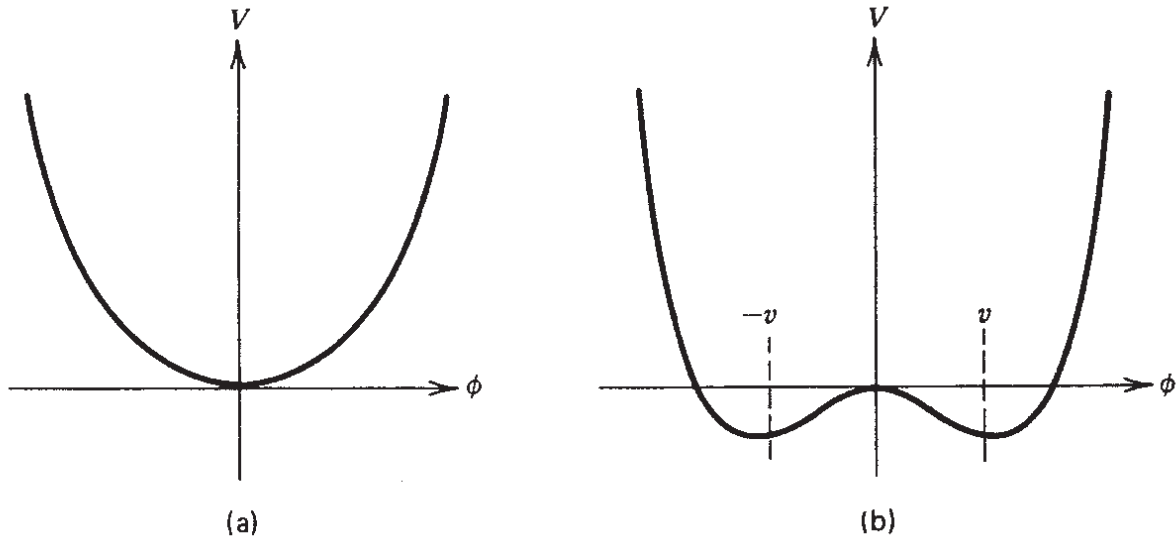


Figure 11.3: The Potential $V(\phi)$ for (a) $\mu^2 > 0$ and (b) $\mu^2 < 0$ and $\lambda > 0$. Source: [1, p. 322].

where $\eta(x)$ is some perturbation around v . Inserting this expansion into the Lagrangian yields

$$\mathcal{L} = \frac{1}{2}(\partial_\mu \eta)^2 - \lambda v^2 \eta^2 - \lambda v \eta^3 - \frac{1}{4} \lambda \eta^4 + \text{const.} \quad (11.27)$$

Here, the first term is a kinetic term for η with mass $m_\eta = \sqrt{2\lambda v^2} = \sqrt{-2\mu^2}$ and the second and third terms are the three-point and four-point interaction terms, respectively.

Two other examples for spontaneous symmetry breaking are

- The alignment of spins in a ferromagnet which violates rotational invariance and
- The bending of an elastic bar under a force aligned with its symmetry axis, see Fig. 11.4.

These examples share the following feature: Variation of some continuous parameter is associated with a transition between two phases with differing degree of symmetry.

Above we considered a discrete symmetry of the Lagrangian; we now turn to the spontaneous breaking of a continuous symmetry, namely of *global* gauge symmetry. Consider now a complex scalar field:

$$\phi = \frac{1}{\sqrt{2}}(\phi_1 + i\phi_2) \quad (11.28)$$

$$\mathcal{L} = (\partial_\mu \phi)^*(\partial^\mu \phi) - \mu^2 \phi^* \phi - \lambda(\phi^* \phi)^2. \quad (11.29)$$

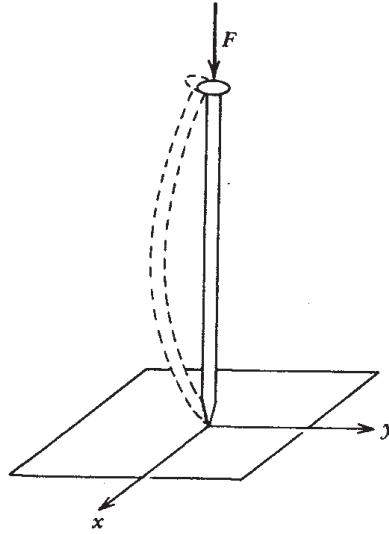


Figure 11.4: *Bending of an elastic bar.* Source: [1, p. 324].

The Lagrangian is invariant under global $U(1)$ transformations $\phi \rightarrow e^{i\alpha}\phi$. In the case $\lambda > 0$, $\mu^2 < 0$ the minimum of the potential $V(\phi)$ is a circle in the ϕ_1 , ϕ_2 plane with

$$\phi_1^2 + \phi_2^2 = v^2 = -\frac{\mu^2}{\lambda}, \quad (11.30)$$

see Fig. 11.5. Out of the infinitely many distinct vacua, degenerate in energy, we choose $\phi_1 = v$, $\phi_2 = 0$. Again, we can expand around the ground state, this time in two orthogonal directions: $\eta(x)$ denotes the perturbation in the steepest ascent direction and $\xi(x)$ is the perturbation in the orthogonal direction (potential valley, see Fig. 11.5):

$$\phi(x) = \frac{1}{\sqrt{2}} [v + \eta(x) + i\xi(x)]. \quad (11.31)$$

Inserting this expansion into the Lagrangian in Eq. (11.29) yields

$$\mathcal{L} = \frac{1}{2}(\partial_\mu \xi)^2 + \frac{1}{2}(\partial_\mu \eta)^2 + \mu^2 \xi^2 + \text{const} + \mathcal{O}((\eta, \xi)^3) \quad (11.32)$$

where we identify a mass term $-1/2m_\eta^2\eta^2$ with $m_\eta = -2\mu^2$ while for the ξ field there is only a kinetic and no mass term.⁴ This is because η is an excitation along the potential direction while ξ corresponds to a rotation along the circle of vacua. Here, the process of spontaneous symmetry breaking leads from a more symmetric phase with two massive fields to a less symmetric phase with a massive and a massless field.

⁴This massless scalar is a Goldstone boson. The Goldstone theorem says that for every broken continuous symmetry there is a massless boson.

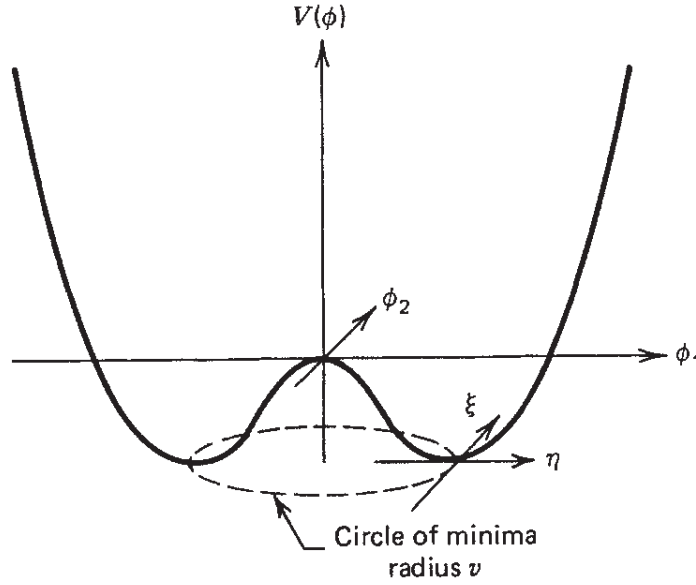


Figure 11.5: The potential $V(\phi)$ for a complex scalar field for the case $\mu^2 < 0$ and $\lambda > 0$. Source: [1, p. 325].

Let us now turn to the spontaneous breaking of *local* gauge symmetry. Consider a complex scalar field and local $U(1)$ gauge transformations:

$$\phi \rightarrow \phi' = \phi e^{ie\alpha(x)}. \quad (11.33)$$

Gauge invariance of the Lagrangian requires the covariant derivative

$$D_\mu = \partial_\mu + ieA_\mu \quad (11.34)$$

with the massless $U(1)$ gauge field A_μ transforming as

$$A_\mu \rightarrow A'_\mu = A_\mu - \partial_\mu \alpha(x). \quad (11.35)$$

A gauge invariant Lagrangian reads

$$\mathcal{L} = (\partial^\mu - ieA^\mu)\phi^*(\partial_\mu + ieA_\mu)\phi - \mu^2\phi^*\phi - \lambda(\phi^*\phi)^2 - \frac{1}{4}F^{\mu\nu}F_{\mu\nu}. \quad (11.36)$$

As before, we consider the case $\mu^2 < 0$, $\lambda > 0$; v and the expansion are

$$v^2 = -\frac{\mu^2}{\lambda} \quad \phi(x) = \frac{1}{\sqrt{2}} [v + h(x)] e^{i\frac{\xi(x)}{v}} \quad (11.37)$$

where in this case we keep the finite rotation due to ξ to preserve gauge freedom. This allows to absorb $\xi(x)$ into a redefinition of the gauge field:

$$A_\mu \rightarrow \hat{A}_\mu = A_\mu - \frac{1}{v}\partial_\mu \xi(x). \quad (11.38)$$

Combining expansion and redefinition with the Lagrangian in Eq. (11.36) yields

$$\mathcal{L} = \frac{1}{2}(\partial_\mu h)^2 - \lambda v^2 h^2 + \frac{1}{2}e^2 v^2 \hat{A}_\mu^2 - \lambda v h^3 - \frac{1}{4}\lambda h^4 + \frac{1}{2}e^2 \hat{A}_\mu^2 h^2 + v e^2 \hat{A}_\mu^2 - \frac{1}{4}\hat{F}^{\mu\nu}\hat{F}_{\mu\nu}. \quad (11.39)$$

The particle spectrum of this theory is as follows.

- There is a massive scalar field h (Higgs) of mass $m_h = \sqrt{2\lambda v^2}$.
- The Goldstone field has been absorbed into \hat{A}_μ and is no longer present in the Lagrangian.
- There is a massive $U(1)$ vector field \hat{A}_μ of mass $m_A = ev$.

It is important to notice that the vacuum state $\phi = v/\sqrt{2}$ is charged under the gauge interaction.

Finally, let us consider the degrees of freedom for the Lagrangian given in terms of ϕ and A and in terms of h and \hat{A} :

\mathcal{L}	Fields	d. o. f.
\mathcal{L} in ϕ, A	ϕ complex, scalar	2
	A^μ massless, spin-1 vector	2
\mathcal{L} in h, \hat{A}	h real, scalar	1
	\hat{A}^μ massive, spin-1 vector	3

This acquiring of a mass by a spin-1 vector boson is also what happens to the photons belonging external fields in superconductors: Since the propagation of the massive photons is exponentially suppressed, the field is correspondingly excluded (Meißner-Ochsenfeld effect).

11.9 Gauge boson masses in $SU(2)_L \times U(1)_Y$

For constructing a gauge invariant Lagrangian, we define the covariant derivative in $SU(2)_L \times U(1)_Y$:

$$D_\mu = \partial_\mu - ig\frac{1}{2}\vec{\tau} \cdot \vec{W}_\mu - ig'\frac{1}{2}YB_\mu. \quad (11.40)$$

The corresponding Lagrangian for a complex scalar field reads

$$\mathcal{L} = [iD^\mu\phi]^\dagger[iD_\mu\phi] - \mu^2\phi^\dagger\phi - \lambda[\phi^\dagger\phi]^2 \quad (11.41)$$

where ϕ is an $SU(2)$ doublet (choose to arrange fields such that $Y = 1$):

$$\phi = \frac{1}{\sqrt{2}} \begin{pmatrix} \phi_1 + i\phi_2 \\ \phi_3 + i\phi_4 \end{pmatrix} = \begin{pmatrix} \phi^+ \\ \phi^0 \end{pmatrix}. \quad (11.42)$$

This is also called a Higgs doublet.

Again let us consider the case $\mu^2 < 0$ and $\lambda > 0$. We may choose the following vacuum state: $\phi_1 = \phi_2 = \phi_4 = 0$ and $\phi_3 = v$ and expand, which, up to a phase, yields

$$v^2 = -\frac{\mu^2}{\lambda} \quad \phi = \frac{1}{\sqrt{2}} \begin{pmatrix} 0 \\ v + h(x) \end{pmatrix}. \quad (11.43)$$

This choice of vacuum breaks the $SU(2)_L$ and $U(1)_Y$ gauge symmetries, since it is hypercharged. The $U(1)_Q$ symmetry of electromagnetism, though, is conserved, because $Q\phi = (T_3 + Y/2)\phi = 0$ and the photon remains massless. What is the particle spectrum for this theory, given the vacuum expectation value chosen above? Inserting $\phi_0 = 1/\sqrt{2}(0, v)^T$ into the relevant term of the Lagrangian in Eq. (11.41), $[D^\mu\phi]^\dagger[D_\mu\phi]$, gives the answer:

$$\begin{aligned} \left| \left(-i\frac{g}{2}\vec{\tau} \cdot \vec{W}_\mu - i\frac{g'}{2}B_\mu \right) \phi \right|^2 &= \frac{1}{8} \left| \begin{pmatrix} gW_\mu^3 + g'B_\mu & g(W_\mu^1 - iW_\mu^2) \\ g(W_\mu^1 + iW_\mu^2) & -gW_\mu^3 + g'B_\mu \end{pmatrix} \begin{pmatrix} 0 \\ v \end{pmatrix} \right|^2 \\ &= \frac{1}{8}v^2g^2 |(W^1)^2 + (W_\mu^2)^2| + \frac{1}{8}v^2(g'B_\mu - gW_\mu^3)(g'B_\mu - gW_\mu^3) \\ &= \left(\frac{1}{2}vg \right)^2 W_\mu^+ W_\mu^{-\mu} + \frac{1}{8}v^2(g'B_\mu - gW_\mu^3)^2 \end{aligned}$$

which, using $Z_\mu = (gW_\mu^3 - g'B_\mu)/\sqrt{g^2 + g'^2}$,

$$= M_W^2 W_\mu^+ W_\mu^{-\mu} + \frac{1}{2}M_Z^2 Z_\mu Z^\mu$$

where

$$\boxed{M_W = \frac{1}{2}vg} \quad \boxed{M_Z = \frac{1}{2}v\sqrt{g^2 + g'^2}}. \quad (11.44)$$

Using $g'/g = \tan\theta_w$ yields the following relation between the W and the Z mass:

$$\boxed{\frac{M_W}{M_Z} = \cos\theta_w}. \quad (11.45)$$

Finally, knowing the W mass, we can use Fermi's constant to obtain an estimate for the vacuum expectation value v :

$$G_F = \frac{\sqrt{2}g^2}{8M_W^2} = \frac{1}{\sqrt{2}v^2} \rightarrow \boxed{v = 246 \text{ GeV}}.$$

11.10 Fermion masses

The usual mass term for quarks and leptons (we focus on the $T_3 = -\frac{1}{2}$ fermions, i.e. down quarks and electrons) takes the form,

$$\mathcal{L}_{m-} = -m\bar{\psi}\psi = -m(\bar{\psi}_R\psi_L + \bar{\psi}_L\psi_R),$$

where ψ_L is a component of the $SU(2)_L$ -doublet χ_L , and ψ_R is an $SU(2)_L$ -singlet. Because of its form, this mass term cannot be invariant under the action of the gauge group $SU(2)_L$ (ψ_R transforms trivially, whereas ψ_L necessarily changes).

The solution consists in pairing ψ_L with an adjoint doublet, the **Higgs doublet**, that we have already introduced earlier to give masses to the vector bosons by means of spontaneous symmetry breaking. A gauge invariant mass term is obtained by coupling to the Higgs doublet, e.g. for the electron (also valid for all $T_3 = -\frac{1}{2}$ fermions):

$$\begin{aligned} \mathcal{L}_{m-} &= -G^e \left[(\bar{\nu}_e \ \bar{e})_L \begin{pmatrix} \phi^+ \\ \phi^0 \end{pmatrix} e_R + \bar{e}_R (\bar{\phi}^+ \ \bar{\phi}^0) \begin{pmatrix} \nu_e \\ e \end{pmatrix}_L \right] \\ &= -\frac{G^e v}{\sqrt{2}} (\bar{e}_L e_R + \bar{e}_R e_L) - \frac{G^e}{\sqrt{2}} h (\bar{e}_L e_R + \bar{e}_R e_L), \end{aligned} \quad (11.46)$$

where G^e denotes the **Yukawa coupling** of the electron, and we used,

$$\begin{pmatrix} \phi^+ \\ \phi^0 \end{pmatrix} = \frac{1}{\sqrt{2}} \begin{pmatrix} 0 \\ v + h(x) \end{pmatrix}.$$

We can now read out of Eq. (11.46),

$$\boxed{m_e = \frac{G^e v}{\sqrt{2}}}, \quad (11.47)$$

and the coupling of the electron to the Higgs field,

$$\text{---} h \text{---} \begin{array}{l} \nearrow e^- \\ \searrow e^- \end{array} = -i \frac{m_e}{v}.$$

Since $m_e = 511$ keV and $v = 246$ GeV, this vertex factor is very small for the electron. In the case of the top, $m_t = 172$ GeV and the vertex factor is much bigger. In the event the Higgs mass is big enough ($m_h > 2m_t$), thus kinematically allowing this decay mode, the branching ratio,

$$BR(h \rightarrow t\bar{t}) = \frac{\Gamma(h \rightarrow t\bar{t})}{\Gamma(h \rightarrow \text{anything})},$$

would be significant.

The vacuum is charged under both $SU(2)_L$ and $U(1)_Y$ but not electrically. Because of this, the photon stays massless, even after $SU(2)_L \times U(1)_Y$ has been broken. Therefore the vacuum expectation value (VEV) of the Higgs fields concentrates on the *neutral* component of the doublet, i.e. the second component having $T_3 = -\frac{1}{2}$ (otherwise the vacuum would also be charged electrically, giving a mass to the photon). Up to now, we have been able to give a gauge invariant mass term to the charged leptons and d -type quarks (d, s, b) all having $T_3 = -\frac{1}{2}$. It appears that we are not able to give a mass term to the neutrinos (neutral leptons) and u -type quarks (u, c, t) having $T_3 = +\frac{1}{2}$ without introducing another Higgs doublet⁵.

In the case of $SU(2)$ (but not in general), we are allowed to use at this end the charge conjugate of the Higgs doublet,

$$\phi^c = i\tau_2\phi^\dagger = \begin{pmatrix} \bar{\phi}^0 \\ -\bar{\phi}^+ \end{pmatrix} \rightarrow \frac{1}{2} \begin{pmatrix} v + h(x) \\ 0 \end{pmatrix}, \quad (11.48)$$

which has $Y = -1$, because ϕ and ϕ^c are equivalent, i.e. can be connected by a unitary transformation.

Example For quarks we get,

$$\begin{aligned} \mathcal{L}_{m-} + \mathcal{L}_{m+} &= -G^d \left[(\bar{u} \ \bar{d})_L \begin{pmatrix} \phi^+ \\ \phi^0 \end{pmatrix} d_R + \bar{d}_R (\bar{\phi}^+ \ \bar{\phi}^0) \begin{pmatrix} u \\ d \end{pmatrix}_L \right] \\ &\quad - G^u \left[(\bar{u} \ \bar{d})_L \begin{pmatrix} \phi^0 \\ -\phi^+ \end{pmatrix} u_R + \bar{u}_R (\bar{\phi}^0 \ -\bar{\phi}^+) \begin{pmatrix} u \\ d \end{pmatrix}_L \right] \\ &= -m_d \bar{d}d - \frac{m_d}{v} h \bar{d}d - m_u \bar{u}u - \frac{m_u}{v} h \bar{u}u. \end{aligned} \quad (11.49)$$

We conclude by emphasising that all fermion masses are generated in a gauge invariant way through coupling of the field to the Higgs VEV v . The coupling of each fermion to the Higgs boson h is proportional to the mass of the particle. The origin of mass is reduced to a Yukawa coupling of the different fermions to the Higgs field.

11.11 Lagrangian of the electroweak standard model

The theory of the electroweak interaction was formulated between 1961 and 1967 by Sheldon Lee Glashow, Abdus Salam and Steven Weinberg. All three received the Physics Nobel Prize in 1979 although the W^\pm and Z^0 had not yet been observed directly. Deep inelastic scattering of spin-polarized electrons off nuclei gave evidence for a minute parity

⁵This is the case in extensions of the standard model, e.g. for the minimal supersymmetric standard model (MSSM), where we have a Higgs doublet for each value of T_3 .

violating interaction (all interactions except the weak interaction conserve parity). The first evidence for neutral currents (mediated by the Z^0 boson) were found in 1973 in the bubble chamber Gargamelle at CERN. Direct observation of both W^\pm and Z^0 was achieved in 1983 by the experiments UA1 also at CERN, leading to the Physics Nobel Prize of 1984 for Carlo Rubbia and Simon van der Meer.

The Lagrangian of the electroweak theory can be decomposed as,

$$\mathcal{L}^{\text{EW}} = \mathcal{L}_{\text{gauge}} + \mathcal{L}_{\text{matter}} + \mathcal{L}_{\text{Higgs}} + \mathcal{L}_{\text{Yukawa}},$$

with,

$$\mathcal{L}_{\text{gauge}} = -\frac{1}{4}\vec{W}_{\mu\nu} \cdot \vec{W}^{\mu\nu} - \frac{1}{4}B_{\mu\nu}B^{\mu\nu} \quad (11.50)$$

$$W_{\mu\nu}^i = \partial_\mu W_\nu^i - \partial_\nu W_\mu^i - ig\varepsilon^{ijk}W_\mu^j W_\nu^k$$

$$B_{\mu\nu} = \partial_\mu B_\nu - \partial_\nu B_\mu,$$

$$\mathcal{L}_{\text{matter}} = \sum_L \bar{L}\gamma^\mu \left(i\partial_\mu + g\frac{1}{2}\vec{\tau} \cdot \vec{W}_\mu + g'\frac{Y}{2}B_\mu \right) L + \sum_R \bar{R}\gamma^\mu \left(i\partial_\mu + g'\frac{Y}{2}B_\mu \right) R, \quad (11.51)$$

$$\mathcal{L}_{\text{Higgs}} = \left| \left(i\partial_\mu + g\frac{1}{2}\vec{\tau} \cdot \vec{W}_\mu + g'\frac{Y}{2}B_\mu \right) \phi \right|^2 - V(\phi), \quad (11.52)$$

$$V(\phi) = -\mu^2\phi^\dagger\phi + \lambda(\phi^\dagger\phi)^2$$

$$\mathcal{L}_{\text{Yukawa}} = -\sum_{f^-} G_-^f (\bar{L}\phi R + \bar{R}\phi L) - \sum_{f^+} G_+^f (\bar{L}\phi^c R + \bar{R}\phi^c L), \quad (11.53)$$

where L denotes a left-handed fermion doublet, R a right-handed fermion singlet, G_\pm^f the fermion Yukawa coupling for $T_3 = \pm\frac{1}{2}$. All terms in \mathcal{L}^{EW} are invariant under $SU(2)_L$ and $U(1)_Y$ gauge transformations.

After the spontaneous symmetry breaking, we have,

$$\phi(x) = \frac{1}{\sqrt{2}} \begin{pmatrix} 0 \\ v + h(x) \end{pmatrix},$$

yielding the masses through the Higgs mechanism:

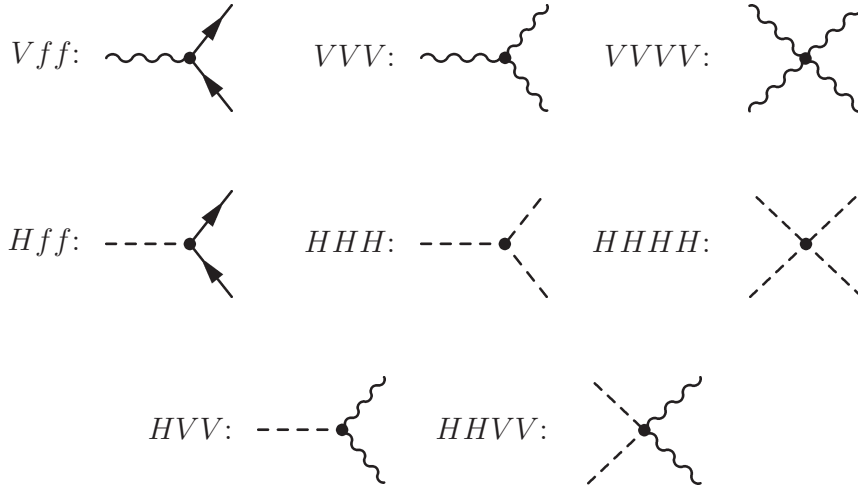
$$M_W = 2gv = 80.4 [\text{GeV}] \quad (11.54)$$

$$M_Z = \frac{M_W}{\cos\theta_w} = 91.19 [\text{GeV}] \quad (11.55)$$

$$M_f = \frac{G^f v}{\sqrt{2}} \quad m_e = 511 [\text{keV}], \dots, m_t = 172 [\text{GeV}] \quad (11.56)$$

$$M_h = v\sqrt{2\lambda} > 114 [\text{GeV}] \quad (\text{LEP}) \quad (11.57)$$

We now classify the vertices of the electroweak Lagrangian (V : vector boson, f : fermion, H : Higgs boson):



Care must be taken in choosing the fields as for example photon can interact with W bosons because they carry an electric charge, but not with the Z boson. All diagrams not involving a Higgs bosons have been observed experimentally so far.

11.12 Properties of the Higgs boson

The decay width of the Higgs boson $\Gamma = \frac{1}{\tau}$ for a two particle final state is (see Eq. (3.15), p. 22),

$$\Gamma_H = \frac{1}{2M_H} \frac{1}{(2\pi)^2} \sum_f \int \frac{d^3p_1}{2E_1} \frac{d^3p_2}{2E_2} \delta^{(4)}(p_f - p_H) |\mathcal{M}_{fH}|^2,$$

where f denotes the final state : $b\bar{b}, t\bar{t}, W^+W^-, Z^0Z^0, \tau^+\tau^-, \dots$ and $m_1 = m_2 = m_f$.

$|\mathcal{M}_{fH}|^2$ cannot depend on individual components of p_1 or p_2 , and we can hence factorize the phase space,

$$R_2 = \int \frac{d^3p_1}{2E_1} \frac{d^3p_2}{2E_2} \delta^{(4)}(p_f - p_H) = \frac{\pi}{2M_H^2} \sqrt{\lambda(M_H^2, m_f^2, m_f^2)} = \frac{\pi}{2} \sqrt{1 - \frac{4m_f^2}{M_H^2}},$$

and hence,

$$\Gamma_H = \frac{1}{16\pi M_H} \sum_f \sqrt{1 - \frac{4m_f^2}{M_H^2}} |\mathcal{M}_{fH}|^2 = \sum_f \Gamma_{H \rightarrow f}. \quad (11.58)$$

We now look at the different final states separately :

Decay into fermions Leptons :

$$\begin{aligned}
 |\mathcal{M}_{lH}|^2 &= \sum_{s,f} \left| \begin{array}{c} f \\ \swarrow \\ \text{---} \bullet \text{---} \\ \searrow \\ \bar{f} \end{array} \right|^2 \\
 &= \frac{m_f^2}{v^2} \text{Tr} \left((\not{p}_f + m_f)(\not{p}_{\bar{f}} - m_f) \right) = \frac{4m_f^2}{v^2} \left(\frac{M_H^2}{2} - 2m_f^2 \right),
 \end{aligned}$$

where s denotes the spin and f the flavour.

Quarks :

$$|\mathcal{M}_{qH}|^2 = \sum_c |\mathcal{M}_{lH}|^2 = 3|\mathcal{M}_{lH}|^2,$$

where c denotes the color.

Plugging these into Eq. (11.58), we get the partial widths,

$$\Gamma_{H \rightarrow l^+ l^-} = \frac{1}{8\pi^2 v^2} m_f^2 M_H \left(1 - \frac{4m_f^2}{M_H^2} \right)^{\frac{3}{2}} \quad (11.59)$$

$$\Gamma_{H \rightarrow q \bar{q}} = \frac{3}{8\pi^2 v^2} m_q^2 M_H \left(1 - \frac{4m_q^2}{M_H^2} \right)^{\frac{3}{2}}. \quad (11.60)$$

We remark at this point that the dominant decay mode (corresponding to the largest partial width) is always into the heaviest kinematically allowed fermion. In the case of a light Higgs boson ($M_H < 2M_{W,Z}$), the dominant channels would be into $b\bar{b}$ and $\tau^+\tau^-$.

The partial width for a decay into fermions is proportional to the mass of the Higgs boson, so there is no upper limit to M_H .

Decay into gauge bosons The relevant vertices are,

$$\begin{array}{cc}
 \begin{array}{c} W_\mu^+ \\ \swarrow \\ \text{---} \bullet \text{---} \\ \searrow \\ W_\nu^- \end{array} & = igM_W g_{\mu\nu}, & \begin{array}{c} Z_\mu^0 \\ \swarrow \\ \text{---} \bullet \text{---} \\ \searrow \\ Z_\nu^0 \end{array} & = \frac{igM_Z}{\cos \theta_w} g_{\mu\nu},
 \end{array}$$

Summing the moduli squared over the polarizations, we get,

$$\sum_{\lambda} \left| \begin{array}{c} \text{---} H \text{---} \\ \bullet \\ \begin{array}{c} \text{wavy line} \\ \text{wavy line} \end{array} \\ \text{---} W^+ \text{---} \\ \text{---} W^- \text{---} \end{array} \right|^2 = g^2 M_W^2 \left(-g^{\mu\rho} + \frac{p_1^\mu p_2^\rho}{M_W^2} \right) \left(-g_{\mu\rho} + \frac{p_{1\mu} p_{2\rho}}{M_W^2} \right) \\ = \frac{g^2 M_H^4}{4M_W^2} \left(1 - 4 \frac{M_W^2}{M_H^2} + 12 \frac{M_W^4}{M_H^4} \right),$$

and an analogous result for the decay $H \rightarrow Z^0 Z^0$. The partial widths are then, respectively,

$$\Gamma_{H \rightarrow W^+ W^-} = \frac{1}{16\pi v^2} M_H^3 \left(1 - \frac{4M_W^2}{M_H^2} \right)^{\frac{1}{2}} \left(1 - 4 \frac{M_W^2}{M_H^2} + 12 \frac{M_W^4}{M_H^4} \right) \quad (11.61)$$

$$\Gamma_{H \rightarrow Z^0 Z^0} = \frac{1}{32\pi v^2} M_H^3 \left(1 - \frac{4M_Z^2}{M_H^2} \right)^{\frac{1}{2}} \left(1 - 4 \frac{M_Z^2}{M_H^2} + 12 \frac{M_Z^4}{M_H^4} \right), \quad (11.62)$$

where the factor $\frac{1}{2}$ in the second line is a symmetry factor for identical bosons.

In the case of a decay into gauge bosons, the partial width is proportional to the third power of the Higgs mass. This implies that for a heavy Higgs boson ($M_H > 2M_{W,Z}$), the decay into gauge bosons will be dominant over the decay into fermions, the only competing fermionic decay being $H \rightarrow t\bar{t}$ (for $M_H \approx 2m_t$). Fig. 10.42(a) and (b), show the different branching ratios and total width as a function of M_H .

Due to this power dependence, one remarks by plugging the known values of M_W , M_Z and v that if $M_H \approx 1$ TeV, $\Gamma_H \approx M_H$ and the interpretation of the Higgs particle as a resonance of the \mathcal{S} -matrix is no longer possible. This yields an upper bound for the Higgs mass in the framework of the standard model. A mass of the order of 1 TeV would imply a coupling $\lambda \approx 1$ requiring some non-perturbative approach (as in QCD for $Q \approx \Lambda^{\text{QCD}}$).

11.13 Tests of electroweak theory

In the previous sections the theory of electroweak interactions was discussed, in particular it was shown how *massive* gauge bosons emerge; in this section we discuss experimental tests of the theory, including the consistency of the standard model parameters, the W and Z boson discovery and measurements of the width. We discuss the forward-backward asymmetries, as well as examples of Higgs boson searches. An introduction to the latter topic is given in Sect. 10.9, here we focus on a specific case study, namely searches for heavy Higgs decaying into W boson pairs.

11.13.1 Parameters of the standard model and historical background

A summary⁶ of the experimental values of the standard model parameters is shown in Fig. 10.1. The stated deviations are a measure for the consistency of the standard model. As can be seen from the bars, which visualize the deviation of the measured from the best fitting values, assuming the standard model to be correct, in units of measurement standard deviations, the majority of the measured parameters is compatible within 1σ . A notable exception is the variable $A_{fb}^{0,b}$, an asymmetry measured in the b sector.

Electroweak unification was accomplished theoretically in the sixties by Glashow, Salam and Weinberg. The predictions derived from this theory were consistent with the observed charged current interactions (flavor-changing exchange of W^\pm bosons, see e. g. Fig. 1.1(b)). However, as we have seen in Sect. 11.5, the theory also predicts neutral current interactions (via Z^0 exchange and γ/Z^0 interference) which had never been observed up to that time. In fact, until 1973 all observed weak interactions were consistent with the existence of only charged bosons W^\pm . The first neutral current interaction was observed at CERN in 1973 with the “Gargamelle” experiment in the following reaction:

$$\nu_\mu + \text{nucleus} \rightarrow \nu_\mu + p + \pi^- + \pi^0$$

which can be explained by a flavor conserving weak interaction, i. e. a weak neutral current. This discovery made urgent the question of how to observe W and Z bosons directly to test electroweak predictions.

11.13.2 W and Z boson discovery, mass and width measurements

Electroweak theory predicted bosons with masses $M_W \sim 83 \text{ GeV}$ and $M_Z \sim 93 \text{ GeV}$. Therefore, to produce W and Z bosons, a particle collider was needed capable of producing particles with mass $\sim 100 \text{ GeV}$. At the time, two candidates were available at CERN. The ISR with $\sqrt{s} = 61 \text{ GeV}$ was too weak and also the SPS, which consisted of a 400 GeV proton beam against a fixed target, did not provide sufficient center of mass energy (recall that for fixed target experiments $\sqrt{s} = \sqrt{2mE}$, see Sect. 4.1.1).

This problem was solved by the $Spp\bar{S}$ machine, designed by Rubbia and van der Meer, a proton-antiproton collider at $\sqrt{s} = 540 \text{ GeV}$. It had a luminosity of $5 \cdot 10^{27} \text{ cm}^{-2}\text{s}^{-1}$, achieved with three against three bunches with $\sim 10^{11}$ particles per bunch. The first collisions took place in 1981.

LEP, which later on delivered part of the precision data discussed in this chapter was an electron-positron collider, while $Spp\bar{S}$ was a hadron collider.⁷ Figure 11.6 shows the

⁶<http://lepewwg.web.cern.ch/LEPEWWG/>

⁷A general comparison of these types of colliders can be found in Sect. 10.1.2.

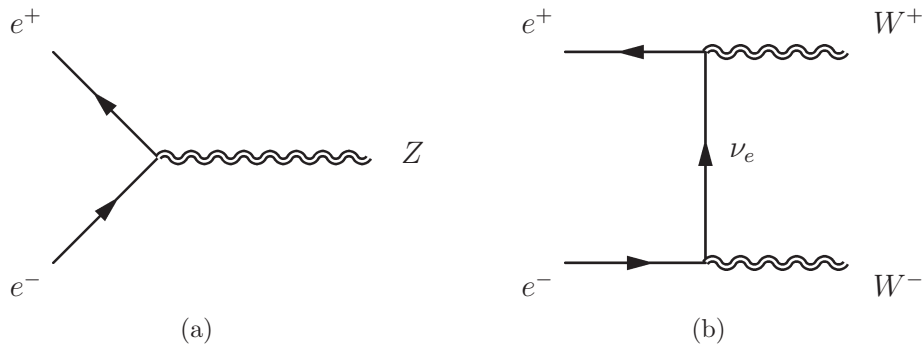


Figure 11.6: Z (a) and W (b) boson production at electron-positron colliders.

relevant production diagrams for e^+e^- colliders while Fig. 11.7 shows a hadron collider production diagram along with the dominant background diagram (see also Fig. 10.14). In the electron-positron case, beam energies of about $M_Z/2$ are sufficient to produce Z bosons (see Fig. 11.6(a)), while W^\pm bosons can only be produced in pairs, requiring a higher center of mass energy (see Fig. 11.6(b)). Now compare this to the hadron collider case shown in Fig. 11.7(a): To produce a Z boson, flavor conservation is required such that processes like $u\bar{u} \rightarrow Z^0$ and $d\bar{d} \rightarrow Z^0$ contribute. The production of W^\pm bosons involves quarks of different flavors, such as $u\bar{d} \rightarrow W^+$ and $\bar{d}u \rightarrow W^-$. What has been said so far concerns *production* of W and Z bosons, what about their *detection*? Consider first the decay into quark-antiquark pairs: The cross section of “usual” two-jet production, e. g. via gluon exchange (see Fig. 11.7(b)) is much larger than the one of hadronic vector boson decays. In other words, the cross section for W production is small compared to the total cross section:

$$\frac{\sigma(\bar{p}p \rightarrow WX \rightarrow e\nu X)}{\sigma_T(p\bar{p})} \simeq 10^{-8}.$$

Therefore, it is preferred to look for W and Z decays into leptons, where the background is smaller:⁸

$$\begin{aligned} W^\pm &\rightarrow e^\pm \nu_e^{(-)}, \mu^\pm \nu_\mu^{(-)}, \tau^\pm \nu_\tau^{(-)} \\ Z^0 &\rightarrow e^+e^-, \mu^+\mu^-, \tau^+\tau^-. \end{aligned}$$

11.13.2.1 W discovery and mass measurement

The UA1 experiment at the $Spp\bar{S}$ collider was an hermetic particle detector optimized for the $W^\pm \rightarrow e^\pm\nu_e/\bar{\nu}_e$ measurement. It featured for the first time the general design principles of collider detectors (see also Sect. 4.3.3): tracking devices inside a magnetic

⁸The Z^0 boson may also decay into neutrino-antineutrino pairs, which makes it possible to determine the number of neutrino families with $m_\nu < M_Z/2$, see below.

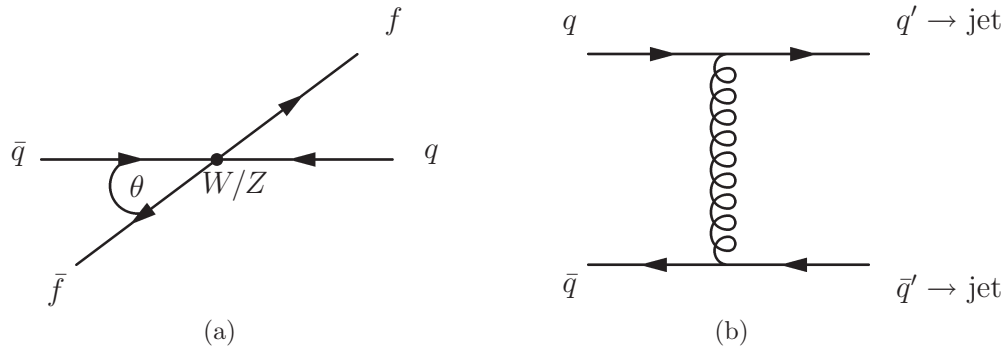


Figure 11.7: (a) Sketch of the kinematics of W and Z boson production at hadron colliders and diagram of a process leading to two jets (b).

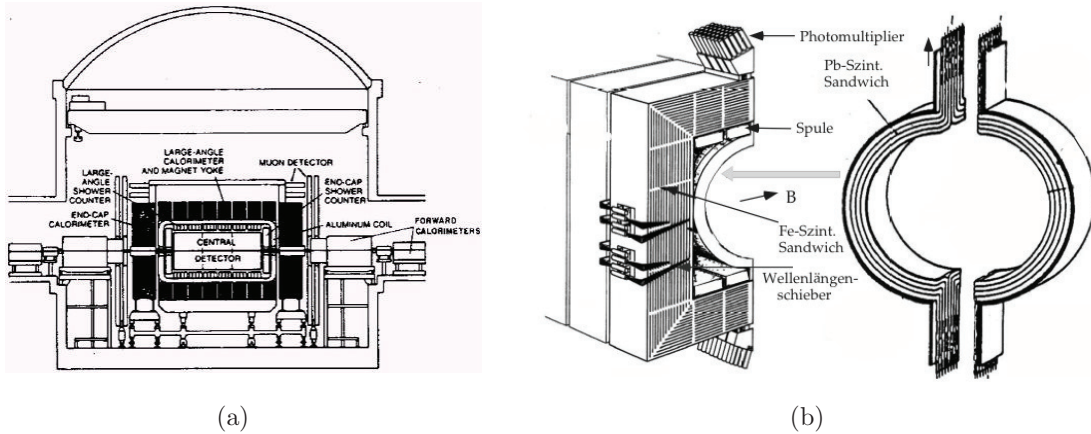


Figure 11.8: *UA1 experiment*. A cross section along the beam line, featuring the important components of collider experiment detectors is shown in (a), while (b) shows the electromagnetic and hadronic calorimeters. Source: [14, p. 305].

field, followed by electromagnetic calorimeters, hadron calorimeters and muon chambers (see Fig. 11.8(a)). Since $M_W \sim 80 \text{ GeV}$, the electromagnetic calorimeter resolution is optimized for 40 GeV electrons to $\pm 500 \text{ MeV} (1\%)$. Because the photomultipliers had to be placed outside the magnetic field of the coil, the hadron calorimeter is sandwiched in the return yoke (see Fig. 11.8(b)): Showering in the lead layers, the particles then produce light in the scintillator layers which is transferred to the photomultipliers via light-guides.

To understand how to search for the W decay in the data, we look at the final-state kinematics. Since the neutrino cannot be detected, there is no direct information on its momentum. However, due to momentum conservation one can write

$$\vec{p}_\perp(\nu) = -\vec{p}_\perp(H) - \vec{p}_\perp(e)$$

where $\vec{p}_\perp(\nu)$ is the neutrino transverse momentum while $\vec{p}_\perp(H)$ and $\vec{p}_\perp(e)$ denote the total hadron transverse momentum and the electron transverse momentum, respectively.

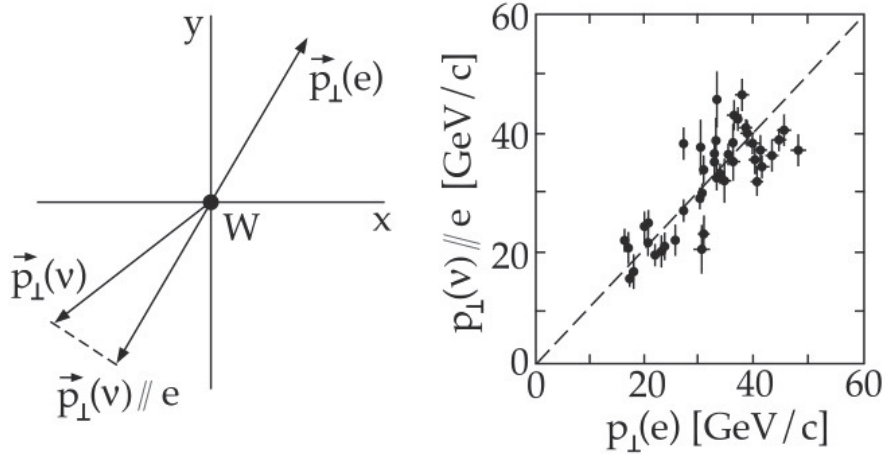


Figure 11.9: *Transverse momenta in a leptonic W decay.* On the LHS one sees a sketch of the electron and neutrino transverse momenta. $\vec{p}_\perp \parallel e$ is the component of the neutrino transverse momentum parallel to $\vec{p}_\perp(e)$. The correlation between these momenta is shown in the RHS Subfig. Source: [14, p. 305].

Momenta are considered in the transverse plane to avoid leakage along the beam lines. Since the W boson is not always produced at rest and the detector resolution is finite, the neutrino transverse momentum $\vec{p}_\perp(\nu)$ is not exactly anti-parallel to the electron transverse momentum (see Fig. 11.9). Nevertheless, there is still a strong correlation between $\vec{p}_\perp(e)$ and the neutrino transverse momentum projected along the electron transverse momentum $\vec{p}_\perp(\nu) \parallel e$ (see Fig. 11.9).

We discuss now how to measure the W boson mass using the electron transverse momentum spectrum (see also exercises). Electron emission is assumed to be isotropic ($dN/d\cos\theta = \text{const}$) and detector effects are emulated with Monte Carlo simulation. One can rewrite the spectrum as

$$\frac{dN}{dp_\perp} = \frac{dN}{d\cos\theta} \frac{d\cos\theta}{dp_\perp} = \text{const} \frac{d\cos\theta}{dp_\perp}$$

where θ is the electron polar angle. Using the kinematics of Sect. 2.1 and $|\vec{p}_\perp| = |\vec{p}| \sin\theta$, we have

$$p_\perp = \frac{M_W}{2} \sin\theta = \frac{M_W}{2} \sqrt{1 - \cos^2\theta},$$

which yields

$$\frac{dp_\perp}{d\cos\theta} = \frac{M_W \cos\theta}{2 \sin\theta} = \frac{M_W}{2} \frac{\sqrt{1 - \sin^2\theta}}{\sin\theta} = \left(\frac{M_W}{2}\right)^2 \frac{\sqrt{1 - \frac{4p_\perp^2}{M_W^2}}}{p_\perp}.$$

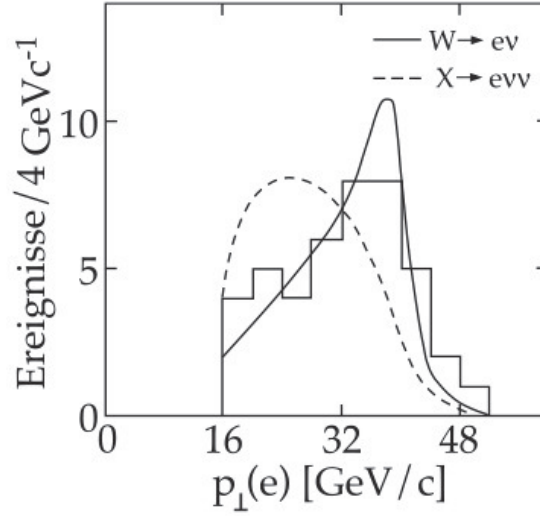


Figure 11.10: *Momentum distribution of the electron perpendicular to the beam (43 events).* The histogram shows the data while the continuous and dashed lines show the Monte Carlo expectation for a two-body decay and three-body decay scenarios, respectively. Source: [14, p. 306].

We thus find

$$\frac{dN}{dp_{\perp}} \propto \frac{p_{\perp}}{\sqrt{M_W^2 - 4p_{\perp}^2}}. \quad (11.63)$$

The denominator vanishes at $M_W = 2p_{\perp}$, which allows to determine the W boson mass from a measurement of the electron transverse momentum spectrum (see Fig. 11.10).

A summary of experimental results for the W boson mass is shown in Fig. 11.11.

11.13.2.2 W and Z width

Using the kinematics discussed Chap. 3, one can calculate the partial width of the W boson. From Eq. (3.15) we have

$$\Gamma = \frac{1}{2M_W} \frac{1}{(2\pi)^2} \int dR_2 |\mathcal{M}_{fi}|^2$$

and Eq. (3.29) reads

$$dR_2 = \frac{1}{8s} \sqrt{\lambda(s, m_e^2, m_\nu^2)} d\Omega.$$

Combining these results yields

$$\frac{d\Gamma}{d\Omega} = \frac{1}{64\pi^2 M_W} |\mathcal{M}_{fi}|^2.$$

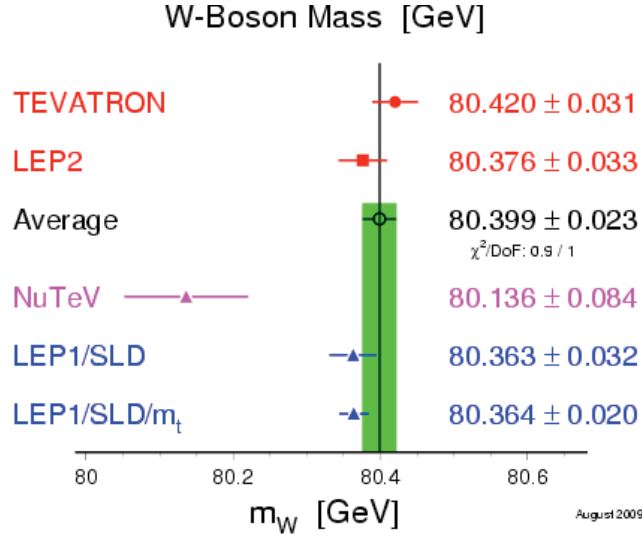


Figure 11.11: *Summary of the current W boson mass measurements.* Source: [17].

Using the following result for the matrix element:

$$|\mathcal{M}_{fi}|^2 = \frac{g^2 M_W^2}{4} (1 - \cos \theta),$$

where θ is the electron polar angle in the center of mass frame, and integrating over θ , one finds for $M_W = 80$ GeV

$$\Gamma(W \rightarrow e\nu) = \frac{g^2 M_W}{48\pi} = \frac{G_F M_W^3}{\sqrt{2} 6\pi} = 224 \text{ MeV}. \quad (11.64)$$

To obtain the total width (for the W^- case) from the partial widths, we consider the following points:

1. All leptonic decays (e , μ , τ) have the same width.
2. $\bar{u}d$ and $\bar{c}s$ are similar to the leptonic channels ($\cos \theta_c \sim 1$).
3. The other hadronic decays ($\bar{u}s$, $\bar{c}d$, $\bar{u}b$, $\bar{c}b$) with quarks of different families are Cabibbo-suppressed.

Keeping these facts in mind, we have to sum over three lepton currents and two quark currents to find the total width Γ_T . Each quark current can be realized in three colors, therefore:

$$\Gamma_T(W) = 3 \text{ lepton currents} + (3 \text{ colors} \times 2 \text{ quark currents}) \quad (11.65)$$

$$= 9\Gamma(W \rightarrow e\nu) = 2.02 \text{ GeV}. \quad (11.66)$$

We now consider the Z boson decay. The Z resonance in the hadronic cross section for e^+e^- annihilation can be used to count the number of neutrino families with $m_\nu < M_Z/2$. One way to accomplish this is to derive a standard model prediction for the Z decay widths as a function of the number of neutrino families N_ν , which can be compared to the experimental data.

First we calculate the partial width of the Z boson decaying into neutrino pairs (see also exercises for the explicit calculation). It can be obtained from the W boson case with some substitutions: Using the Feynman rules given in Sect. 11.7, one finds, since $c_V^\nu = c_A^\nu = 1/2$, that substituting

$$g \rightarrow \frac{g}{\sqrt{2} \cos \theta_w}, \quad M_W \rightarrow M_Z$$

in the partial W width in Eq. (11.64) does the trick:

$$\Gamma(Z \rightarrow \nu\bar{\nu}) = \frac{g^2 M_Z}{96\pi \cos^2 \theta_w} = \frac{G_F M_Z^3}{\sqrt{2} 12\pi} = 165 \text{ MeV}, \quad (11.67)$$

assuming $M_Z = 91 \text{ GeV}$. To obtain the total width of the Z boson, one has to sum over all partial widths, originating from all the allowed decays into quarks and leptons. Solving exercise sheet 9⁹ we showed that for the general fermionic case the Z partial width is

$$\Gamma(Z \rightarrow f\bar{f}) = \frac{g^2}{48\pi \cos^2 \theta_w} \sqrt{M_Z^2 - 4m_f^2} \left\{ [c_V^f]^2 \left(1 + \frac{2m_f^2}{M_Z^2} \right) + [c_A^f]^2 \left(1 - \frac{4m_f^2}{M_Z^2} \right) \right\}.$$

Neglecting m_f , one finds that the total Z width is proportional to the sum

$$\sum_{\substack{\text{fermions} \\ m_f < M_Z/2}} \left([c_V^f]^2 + [c_A^f]^2 \right)$$

which can be calculated using Tab. 11.3. Note that only the following fermionic final states contribute:

- three neutrino pairs: $\nu_e\bar{\nu}_e$, $\nu_\mu\bar{\nu}_\mu$, $\nu_\tau\bar{\nu}_\tau$;
- three other halves of the doublets: e^+e^- , $\mu^+\mu^-$, $\tau^+\tau^-$;
- two quark pairs with $T_3 = +1/2$: $u\bar{u}$, $c\bar{c}$ and finally
- three quark pairs with $T_3 = -1/2$: $d\bar{d}$, $s\bar{s}$, $b\bar{b}$.

Assuming $\sin^2 \theta_w = 0.23$, the total Z width is

$$\Gamma_T(Z) = \frac{g^2 M_Z}{48\pi \cos^2 \theta_w} \sum_{\substack{\text{fermions} \\ m_f < M_Z/2}} \left([c_V^f]^2 + [c_A^f]^2 \right) = 2.41 \text{ GeV}.$$

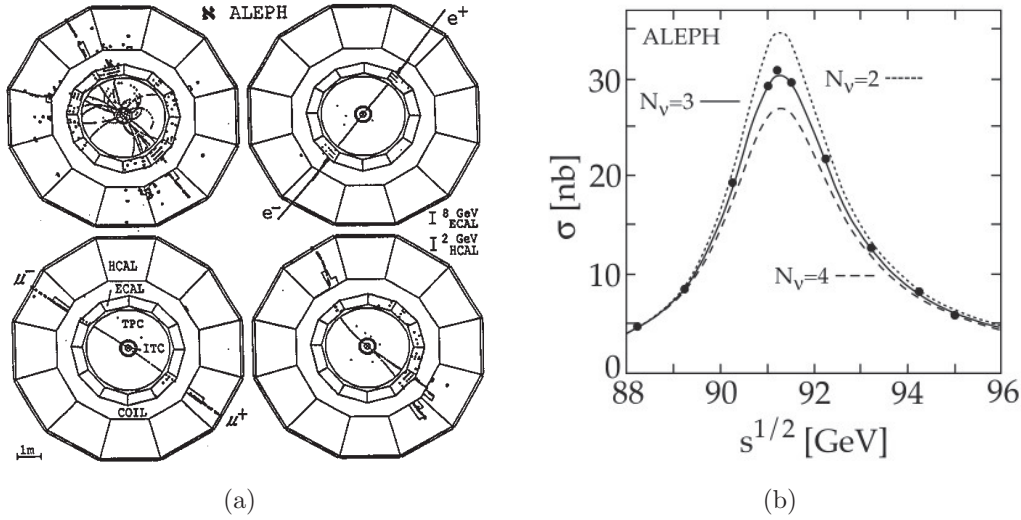


Figure 11.12: *ALEPH event displays of Z decays and Z jets cross-section as function of \sqrt{s} .* Subfigure (a) shows typical events in the ALEPH detector. Starting in the top left corner and proceeding in clockwise order, one has $e^+e^- \rightarrow$ hadrons, $e^+e^- \rightarrow e^+e^-$, $e^+e^- \rightarrow \mu^+\mu^-$ and $e^+e^- \rightarrow \tau^+\tau^-$. Source: [15, p. 15]. The Z cross section fit is shown in (b). The dots show the measurement while the expectation from scenarios with different number of neutrino families are shown by the continuous and dashed lines. Source: [14, p. 312].

One can measure the hadronic cross section for e^+e^- annihilation around the Z peak as a function of \sqrt{s} to constrain the number of neutrino families. This is done by a fit to a modified Breit-Wigner distribution,

$$\sigma(s) = \frac{12\pi\Gamma(e^+e^-)\Gamma(f\bar{f})}{M_Z^2} \frac{s}{(s - M_Z^2)^2 + M_Z^2\Gamma_T^2(Z)}, \quad (11.68)$$

for the Z resonance. One also has to take into account γ/Z interference, the $1/s$ dependent QED contribution, and quite substantial corrections due to initial and final state radiation. To measure the relevant cross sections, one selects (e.g. hadronic) events, which is done using on their basic properties, such as number of tracks (see Fig. 11.12(a)). Since the cross section is given by $\sigma = N/(\varepsilon\mathcal{L}_{\text{int}})$, the precision of the result depends on the precision of the integrated luminosity measurement, as well as the trigger and its efficiency. A best fit to the hadronic cross section yields for the number of light neutrino families

$$N_\nu = 2.994 \pm 0.012$$

(see Fig. 11.12(b)). Note that because of the kinematics of $1 \rightarrow 2$ decay, this does not exclude heavy ($m_\nu > M_Z/2$) quark and neutrino families.

As we have seen, since the cross section is inversely proportional to the integrated luminosity, the luminosity error propagates into the cross section error. Therefore, it is essential

⁹http://www.itp.uzh.ch/~pfmonni/PPPII_FS10/sheet9.pdf

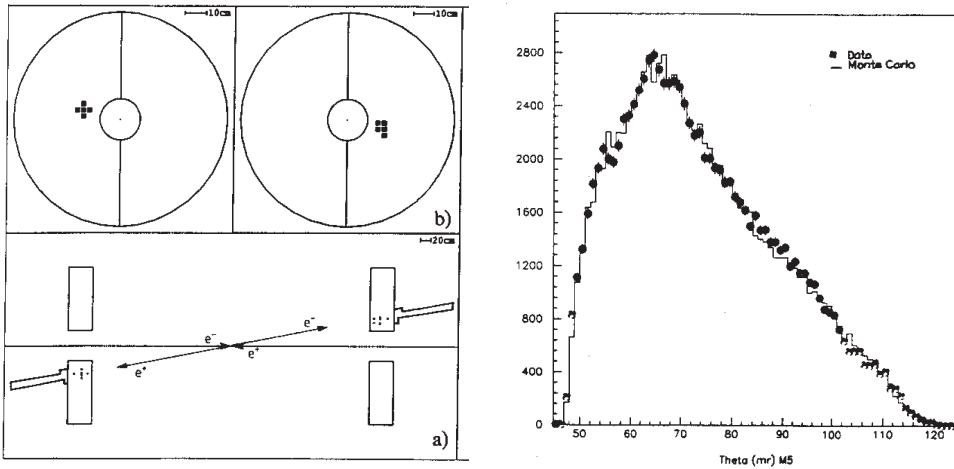


Figure 11.13: *Luminosity measurement in ALEPH using the Bhabha scattering.* On the left a small angle electron-positron scattering event is shown. (a) shows a cut including the beam direction and (b) is a view along the beam of the two luminosity calorimeters. A comparison of measured and simulated polar angle of the scattered electron is shown on the right. Source: [15, p. 20].

to determine the luminosity with high accuracy. This is done by measuring the rate of Bhabha scattering, which can be precisely calculated. As we have seen in Sect. 6.2.4, the corresponding cross section is divergent as the electron polar angle goes to zero (see also Fig. 11.13). This procedure yields a final precision of about 3% for the luminosity measurement.

Selecting leptonic events, one can perform the same measurement as the one shown for the hadronic case (see Fig. 11.14(a); note that the cross sections are considerably smaller). This delivers the partial widths $\Gamma(l\bar{l})$ and thus allows for a test of lepton universality. Remembering our discussion of the total Z width, one finds for the leptonic widths (e. g. for muons) the following prediction:

$$\frac{\Gamma(\mu^+\mu^-)}{\Gamma_T} = \frac{[c_V^\mu]^2 + [c_A^\mu]^2}{\sum_{m_f < M_Z/2}^{\text{fermions}} ([c_V^f]^2 + [c_A^f]^2)} = 3.4\%.$$

The corresponding experimental result is

$$\frac{\Gamma(\mu^+\mu^-)}{\Gamma_T} = (3.366 \pm 0.007)\%.$$

A summary of the LEP results for the Z boson width is shown in Fig. 11.14(b). To conclude this section, let us put our discussion into an historic and energetic context: Figure 11.15 shows the cross section for $e^+e^- \rightarrow \text{hadrons}$ as measured by various experiments at center of mass energies up to 200 GeV. For center of mass energies smaller than about 50 GeV, the

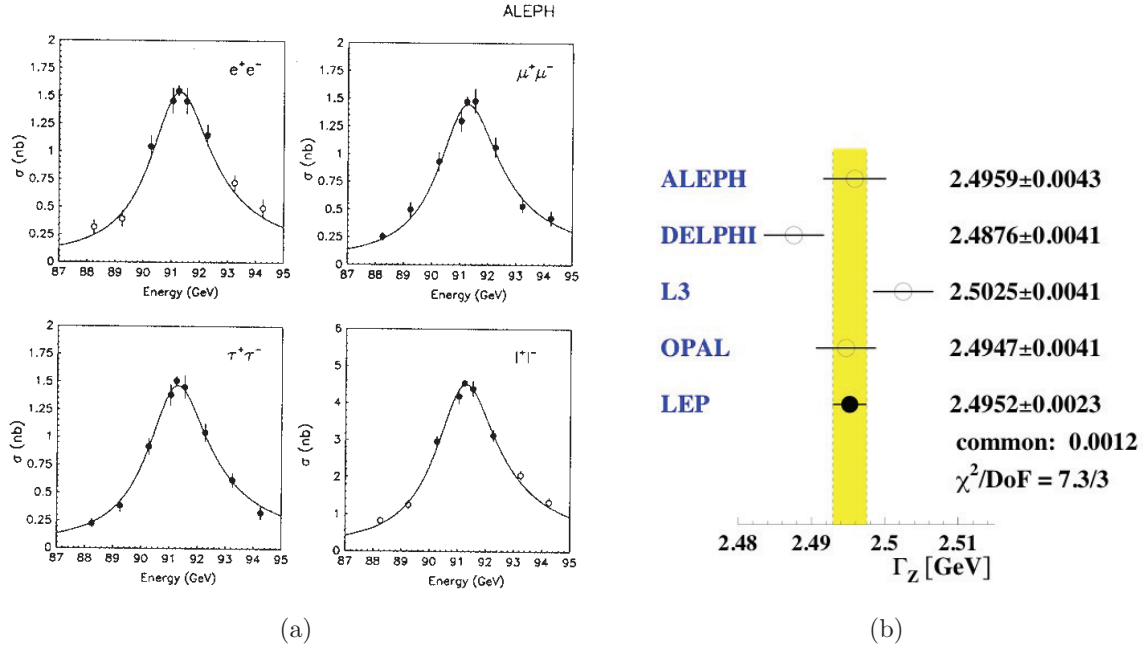


Figure 11.14: Cross sections for electron-positron annihilation into leptons around the Z pole measured by ALEPH (a) and LEP summary of the Z width measurements (b). Source: [15, p. 24].

cross section agrees with the $1/s$ prediction obtained by QED alone (quark mass effects included, see Sect. 8.1). Around 90 GeV the Z resonance is the dominant contribution. The figure shows also the cross section for W production from $e^+e^- \rightarrow W^+W^-$.

11.13.3 Forward-backward asymmetries

As we have begun to discuss in Sect. 6.2.5, the weak contributions to electron-positron annihilation cross sections result in forward-backward asymmetries (in the angle between the outgoing fermion and the incident positron), which are not predicted by QED alone (see e. g. Fig. 6.17). Solving exercise sheet 8¹⁰, we showed that the differential cross section for $e^+e^- \rightarrow f\bar{f}$, obtained by squaring the sum of the γ and the Z exchange diagram, can be written as

$$\frac{d\sigma_f}{d\Omega} = \frac{\alpha^2 N_c^f}{4s} [F_1(s)(1 + \cos^2 \theta) + 2F_2(s) \cos \theta] \quad (11.69)$$

where

$$\begin{aligned} F_1(s) &= Q_f^2 - 2v_e v_f Q_f \text{Re}\chi + (v_e^2 + a_e^2)(v_f^2 + a_f^2)|\chi|^2 \\ F_2(s) &= -2a_e a_f Q_f \text{Re}\chi + 4v_e a_e v_f a_f |\chi|^2 \end{aligned}$$

¹⁰http://www-theorie.physik.unizh.ch/~pfmonni/PPPII_FS10/sheet8.pdf

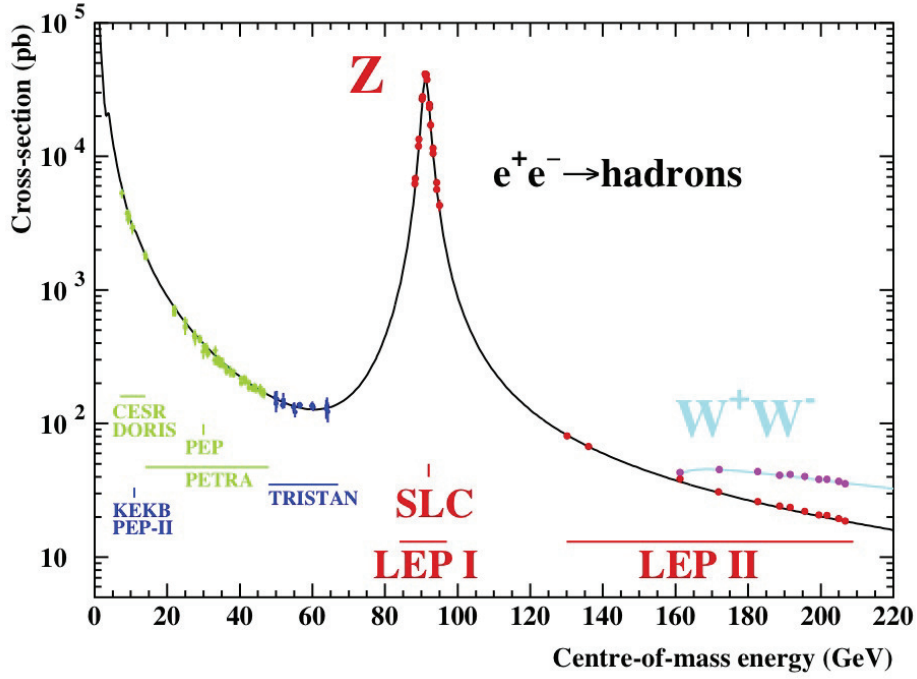


Figure 11.15: Summary of the $e^+e^- \rightarrow \text{hadrons}$ cross section measurements as a function of the center of mass energy \sqrt{s} .

with

$$\chi = \frac{s}{s - M_Z^2 + iM_Z\Gamma_T(Z)}$$

the Breit-Wigner term (compare Eq. (11.68)) and

$$v_f \equiv \frac{c_V^f}{2 \sin \theta_w \cos \theta_w}$$

$$a_f \equiv \frac{c_A^f}{2 \sin \theta_w \cos \theta_w}.$$

To get a quantitative estimate of the forward-backward asymmetry, we define the following quantity

$$A_{\text{FB}} = \frac{\mathcal{I}(0, 1) - \mathcal{I}(-1, 0)}{\mathcal{I}(0, 1) + \mathcal{I}(-1, 0)} \quad (11.70)$$

where we have defined the integral $\mathcal{I}(a, b)$ as

$$\mathcal{I}(a, b) \equiv \int_a^b d \cos \theta \frac{d\sigma}{d \cos \theta}. \quad (11.71)$$

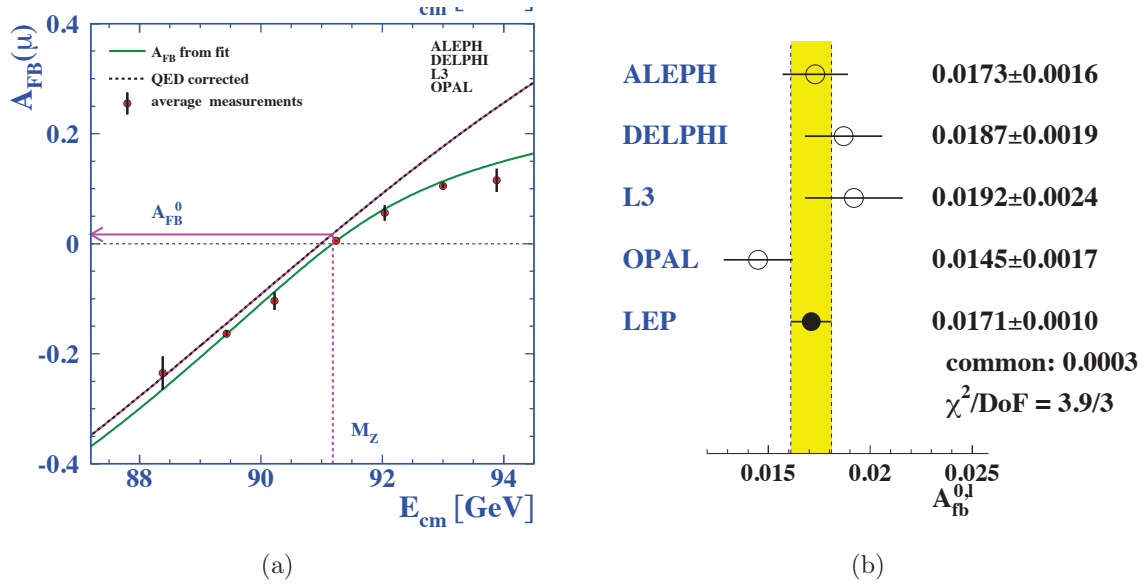


Figure 11.16: *LEP results for forward-backward asymmetry A_{FB} .* (a) shows a plot of the LEP data for A_{FB} as a function of \sqrt{s} and (b) shows a summary of the numerical values at $\sqrt{s} = M_Z$ and the combined result.

Thus forward-backward asymmetry means $A_{FB} \neq 0$. In terms of F_1 , F_2 defined above, we have

$$A_{FB} = \frac{3 F_2}{4 F_1} = \frac{3v_e a_e v_f a_f}{(v_e^2 + a_e^2)(v_f^2 + a_f^2)} = 3 \frac{(v/a)_e (v/a)_f}{[1 + (v/a)_e^2][1 + (v/a)_f^2]}. \quad (11.72)$$

Therefore, at the Z peak the asymmetry A_{FB} is sensitive to the ratio of vector to axial vector couplings $v/a = c_V^f/c_A^f$. Recalling the definition of c_V^f and c_A^f (see Sect. 11.7), we see that in the electroweak theory the c_V/c_A ratio depends on $\sin^2 \theta_w$:

$$c_V/c_A = 1 - 4|Q| \sin^2 \theta_w. \quad (11.73)$$

Furthermore, rewriting Eq. (11.69) using Eq. (11.72) yields

$$\frac{d\sigma}{d\cos\theta} \propto 1 + \cos^2\theta + \frac{8}{3} A_{FB} \cos\theta \quad (11.74)$$

(see Fig. 6.17). Figure 11.16(a) shows results for A_{FB} by the four LEP experiments. The corresponding numerical values are shown in Fig. 11.16(b). Combining these results gives

$$A_{FB} = 0.0171 \pm 0.0010$$

for the forward-backward asymmetry at $\sqrt{s} = M_Z$.

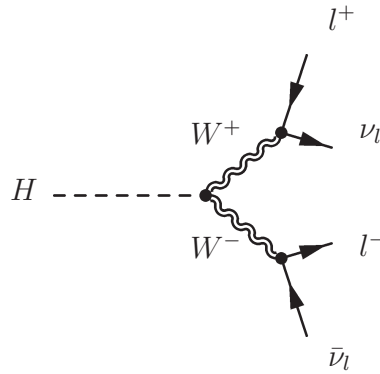


Figure 11.17: *Feynman diagram for the decay of a heavy Higgs into a W^+W^- pair.*

11.13.4 Searches for heavy Higgs decays into W pairs

Having studied extensively the observable consequences of non-vanishing gauge boson masses, we now turn to the source of this phenomenon. In Sect. 11.12 we discussed properties of the Higgs boson, including its partial widths for decay into W and Z boson pairs. Sect. 10.9 introduces the principles of Higgs production and searches; here we focus on searches of heavy Higgs in the the $H \rightarrow W^+W^-$ channel.

Recall from Sect. 10.9 that for $m_H \simeq 140-175$ GeV the important Higgs discovery channel is $H \rightarrow W^+W^-$, which yields two leptons and missing transverse energy in the final state (see Fig. 11.17).

Figure 11.18 shows the orders of magnitude of various production cross sections at Tevatron. Note the difference of about ten orders of magnitude between the production cross sections for heavy flavors and Higgs bosons. In addition, also the production cross sections for Z/γ^* and standard model W^+W^- pair production not involving Higgs boson exchange are orders of magnitude larger than the Higgs production cross section.

How does one select events in the desired final states? To reduce the background as much as possible, the following cuts are applied:

- *Total missing energy larger than 20 GeV.*
This requirement reduces the $Z/\gamma^* \rightarrow$ leptons background.
- *Invariant mass of two leptons larger than 15 GeV.*
This requirement reduces the background from semi-leptonic decays of heavy quarks.

The remaining background is due to standard model W pair production not involving Higgs bosons (see Fig. 11.19). Therefore, the remaining task is to reject this kind of electroweak background obscuring the $H \rightarrow W^+W^-$ signal. To achieve this aim, one can exploit the fact that the standard model Higgs is a scalar (i. e. it has spin 0). W bosons, on the other hand, have spin 1. To conserve angular momentum, the two decay leptons

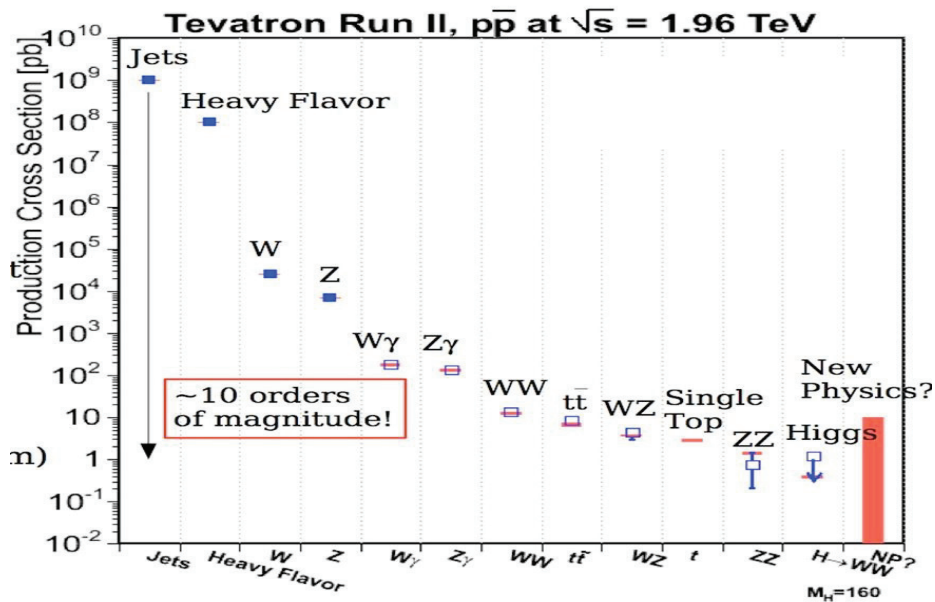


Figure 11.18: Various production cross sections at Tevatron. Note that the scale is logarithmic.

are almost collinear. Therefore, it is convenient to measure the opening angle between the lepton pair in the transverse plane, $\Delta\phi_{l+l^-}$. This allows to select only events with small opening angle: $\Delta\phi < 2$ rad. Figure 11.20 shows plots for the ee , $\mu\mu$ and $e\mu$ case: The left column shows the signal plus a considerable amount of background by various processes unrelated to Higgs production. The right column shows $\Delta\phi$ after all cuts but the $\Delta\phi < 2$ cut are applied (the $\Delta\phi$ cut is indicated by arrows). If no event survives all cuts, it is possible to set an exclusion limit on the Higgs mass. A combined Tevatron (DØ and CDF) result using an amount of data corresponding to $\mathcal{L}_{\text{int}} \sim 5 \text{ fb}^{-1}$ excluding the mass range from 162 to 166 GeV at 95% CL is shown in Fig. 11.21. The current combined Tevatron and LEP standard model Higgs mass fit and excluded regions¹¹ are shown in Fig. 10.2.

¹¹<http://lepewwg.web.cern.ch/LEPEWWG/>

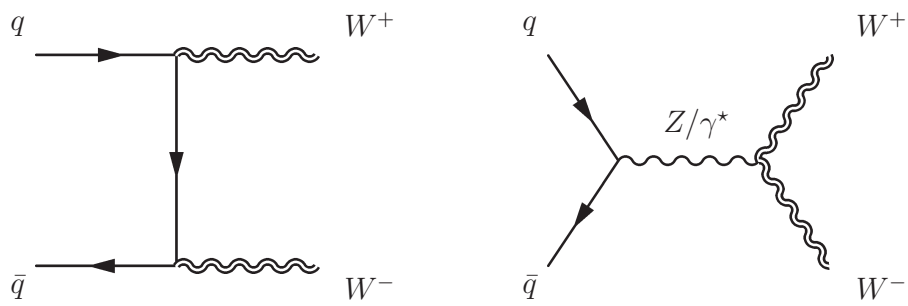


Figure 11.19: *Examples of W^+W^- production diagrams at hadron colliders not involving Higgs boson exchange.*

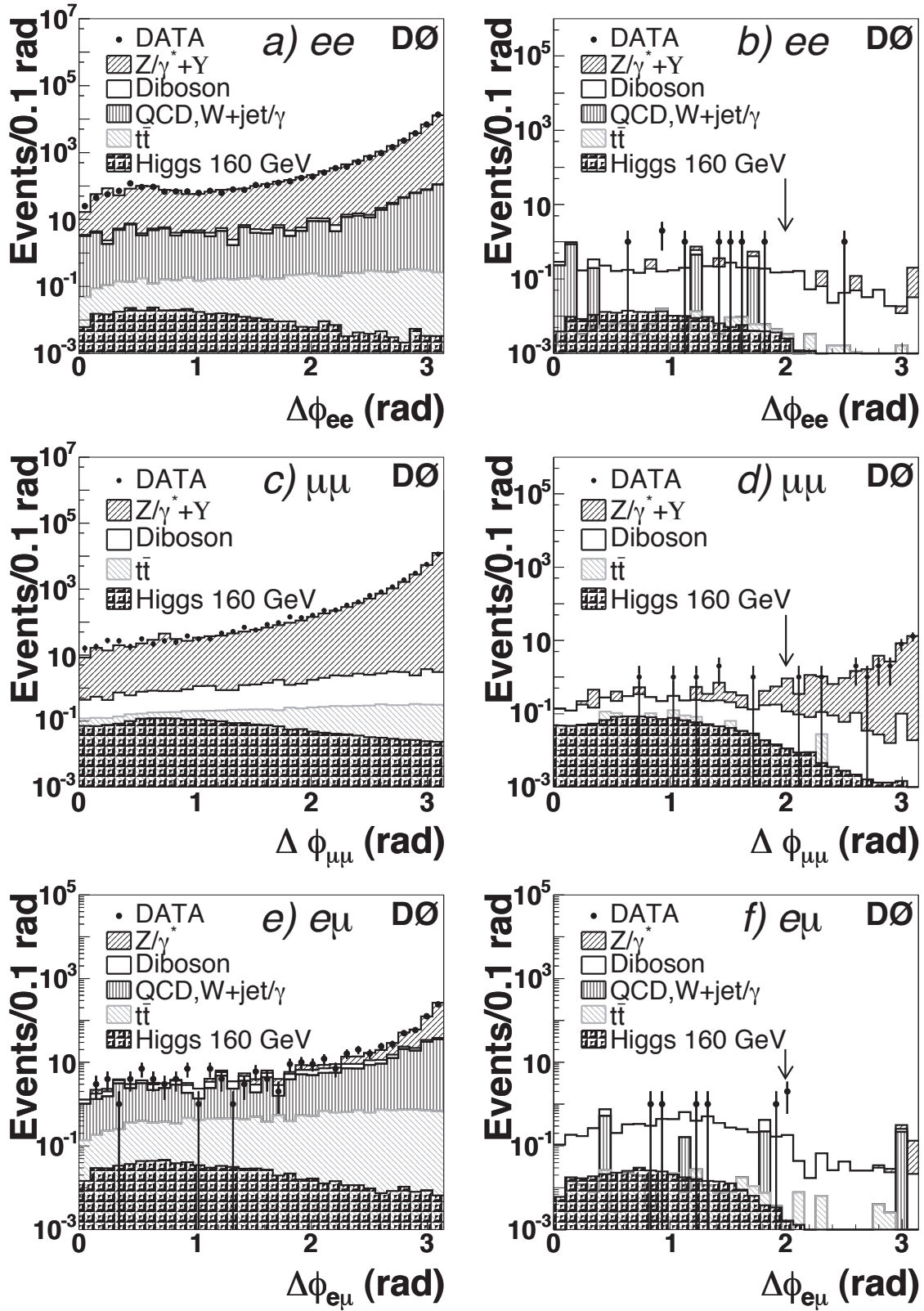


Figure 11.20: Distribution of the opening angle $\Delta\phi_{l\bar{l}}$ after applying the initial transverse momentum cuts (a), (c), (e) and after all cuts, except for the $\Delta\phi$ cut (b), (d), (f). Source: [18].

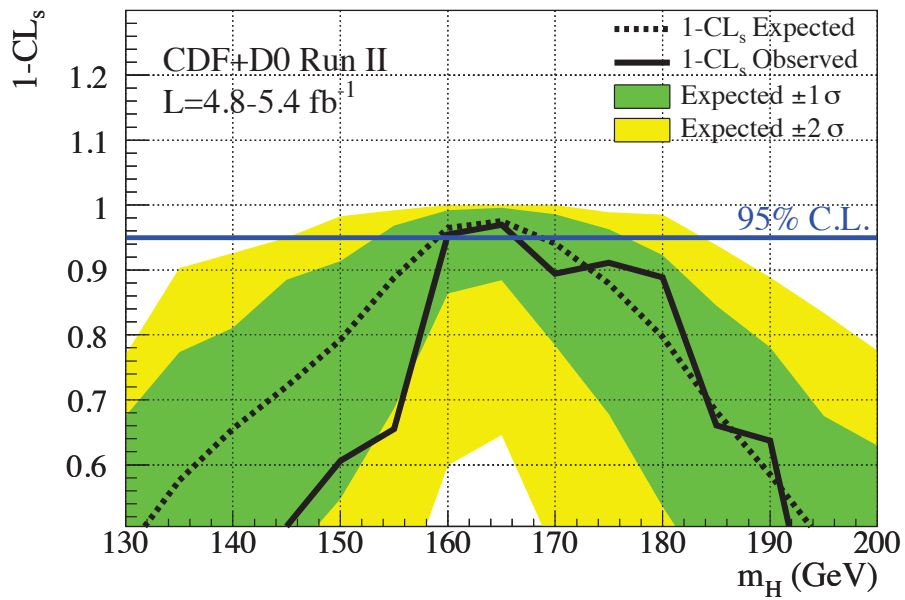


Figure 11.21: *Higgs mass range exclusion with combined Tevatron results.* Source: [19].